

Electrosprays in the cone-jet mode: from Taylor cone formation to spray development

Joan Rosell-Llompart ^{a,b}, Jordi Grifoll ^b, Ignacio G. Loscertales ^c

^a Catalan Institution for Research and Advanced Studies - ICREA, E-08010 Barcelona, Spain

^b Department of Chemical Engineering, Universitat Rovira i Virgili, E-43007 Tarragona, Spain

^c Escuela de Ingenierías Industriales, Universidad de Málaga, E-29071 Málaga, Spain

Abstract

Electrospray is a relatively mature research field, with sustained and growing activity. It has attracted researchers from diverse application fields. Electrospray is perhaps best known as a tool which has enabled the mass spectrometry analysis of large biomolecules (proteins and DNA). It has also been proposed as a colloidal thruster for spacecraft propulsion. And also, it has been used as a general methodology for converting precursor droplets to microspheres and other particle morphologies and films, with controlled nanostructure. In parallel to this body of applied research, other efforts have been aimed at improving the understanding of the underlying physics of electrosprays. While many reviews exist on applications of this system, wherein the physics of the process is described to a certain extent, the present review focuses on the fundamentals. We begin by describing the different modes developing in liquid menisci to which an electrical potential is applied. Due to its applications, the mode of greatest interest is the cone-jet mode in which a steady microscopic jet is emitted and breaks up periodically into uniformly sized droplets. The physics of this mode is then explored in detail, first by reviewing the remarkable effort in the field aimed at identifying so called scaling laws. These are simple scaling relationships connecting the variables of the problem which can be applicable to many operating conditions. We then describe the dynamics of generation of the jet which emerges from the electrified conical meniscus, as well as the physics associated with the spray plume development. We conclude with the extension of these concepts to multi-fluid configurations, such as coaxial and parallel flows.

Keywords: electrospray; EHDA; cone-jets; coaxial electrospraying; charged droplets; electrohydrodynamic modes

1. Introduction

Electrohydrodynamic atomization (EHDA) of liquids refers to the fine fragmentation of liquids caused by electrostatic stresses, and it is synonymous with *electrohydrodynamic spraying* and *electrospraying*. The latter term was probably invented in the 60's in the context of preparation methods of thin nuclear targets (Verdingh & Lauer, 1964; Shorey & Michelson, 1970), and was later re-introduced by Yamashita & Fenn (1985), while *electrohydrodynamic spraying* was used by Pfeifer & Hendricks (1968), by Hayati et al. (1987) and by Cloupeau & Prunet-Foch (1989), while EHDA was introduced by Smith (1986) and re-introduced later by Grace & Marijnissen (1994). Electrospraying occurs when a liquid is subjected to a high electrostatic potential relative to its surroundings and, as a result, develops a pointed meniscus which ejects a liquid micro-jet, whose breakup produces charged droplets (Fig. 1a). Usually, the above terms are used to the situation wherein the pointed menisci, also called Taylor cones, and the ensuing jets are stationary.

The development of *transient* jets when liquid bodies were electrified was well known to Rayleigh (1882), who developed the first linear stability analysis of an electrified droplet. He assumed idealized conditions, but his calculation of the critical charge level has become a widely used result (Saville, 1997; Fernández de la Mora, 2007). The so-called *Rayleigh breakup* of a charged droplet has only recently been captured by high speed video (Achtzehn et al., 2005), although they had been photographed before (Fig. 1b). The instability evolves by development of a prolate shape which forms two pointed ends, with emission of two opposed jets, which are called *Rayleigh jets*. A similar instability happens to a neutral droplet under the action of a strong DC field (Saville, 1997) (Fig. 1c).

Electrospray is a relatively mature research field, with sustained and growing activity. It has attracted researchers from diverse application fields. Electrospray is perhaps best known as a tool which has enabled the mass spectrometry analysis of large biomolecules (proteins and DNA) (Fenn, 2003). It has also been proposed as a colloidal thruster for spacecraft propulsion (Velásquez-García et al., 2006). It has also been used as a general methodology for converting precursor droplets to microspheres and other particle morphologies and films, with controlled nanostructure (Okuyama & Lenggoro, 2003; Jaworek, 2007a, 2007b; Jaworek & Sobczyk, 2008; Yurteri et al., 2010; Bock et al., 2012; Xie et al., 2015; Nguyen et al., 2016).

In parallel to this body of applied research, other efforts have been aimed at improving the understanding of the underlying physics of electrosprays. Since the studies conducted by John Zeleny at Yale University early in the 20th century (Zeleny, 1907, 1914, 1915, 1917, 1920, 1935), the fundamental studies on electrosprays were interrupted during the WWII, and later restarted with key contributions, e.g. the famous G. I. Taylor's analysis of the electro-hydro-static equilibrium of conical menisci (1964, 1969). During the Space Age (60's and 70's) the field underwent a rebirth with the search for new spacecraft propulsion methods (as reviewed by López-Urdiales, 2004). In the late eighties, the discovery of the electrospray-based method for ionizing biomolecules in John B. Fenn's lab (also at Yale) (Fenn et al., 1989) attracted the interest of more researchers (Fenn's colleagues like Juan Fernández de la Mora, and Alessandro Gomez; and others elsewhere, like Antonio Barrero from Universidad de Sevilla and Jan Marijnissen at TU Delft). Thus, a program to understand the fluid mechanics of steady cone-jet structures, got started with an aim to predict the behavior of cone-jets from first principles. To this day, this program has attracted many other researchers, having accumulated hundreds of contributions by groups worldwide.

While many reviews exist on applications of this system, wherein the physics of the process is described to a certain extent, the present review focuses on the fundamentals.

The structure of this review is as follows: We start by describing the different fluid dynamic modes adopted by liquid menisci to which an electrical potential is applied (section 2). Due to its applications, the mode of greatest interest is the cone-jet mode, wherein the liquid meniscus emits a steady microscopic jet, which breaks up periodically into uniformly sized droplets. We focus on this mode in Section 3, where its physics is explored in detail, first by reviewing the remarkable effort which has been made in the field towards identifying so-called *scaling laws*. These are simple scaling relationships connecting the variables of the problem, which are applicable to different physicochemical liquid properties and operating conditions. We then describe the dynamics of generation of the jet that emerges from the electrified conical meniscus, as well as the physics associated with the spray structure development. In section 4, we extend these concepts to multi-fluid configurations, such as coaxial and parallel flows.

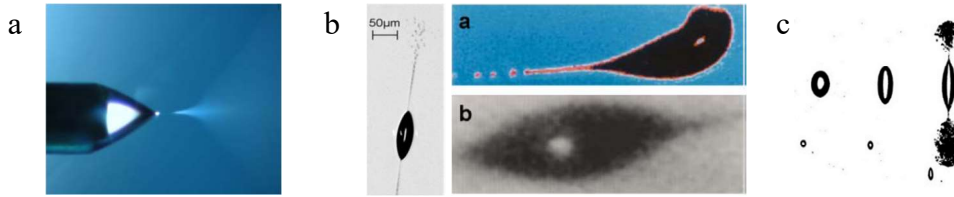


Fig. 1. Examples of electro-spraying from Taylor cones. (a): Liquid meniscus at a cylindrical tube end in the cone-jet mode, producing a spray. (b): Transient Taylor cone forms during Rayleigh instability (Achtzehn et al., 2005; Gomez & Tang, 1994) (c): Three stages (L to R) of the electro-capillary instability of a neutral water droplet in hydrocarbon oil, subject to a vertical DC electrical field (Garton & Krasucki, 1964).

2. Principle of electrohydrodynamic spraying and modes

A liquid drop emerging from a nozzle displays, under the action of surface tension and accelerating forces (e.g. gravitational and/or electrical), a range of oscillating and non-oscillating behaviors, broadly known as dripping and jetting modes. Over the years, the various electro-hydrodynamic modes have been classified (Cloupeau & Prunet-Foch, 1990; Grace & Marijnissen, 1994; Juraschek & Röllgen, 1998; Jaworek & Krupa, 1999; Marginean et al., 2007; Verdoold et al., 2014). Identifying all possible modes and understanding their underlying physics is an ongoing challenge, although considerable progress has been made since the development of high speed video and fast electrical current measurements (Verdoold et al., 2014). The aim of this section is to provide objective criteria to differentiate the various modes. We also describe parametric operation windows by reference to dimensionless numbers.

2.1. Relevant independent parameters and some dimensionless numbers

We consider here a liquid meniscus (or pendant drop) of diameter D emerging from an electrified (downward facing) long tube of inner diameter D_I and outer diameter D_O . The liquid is supplied through it at a constant volumetric flow rate Q (either by using a pump or from a pressurized container by a supply line which provides enough hydrodynamic resistance, such that the pressure drop along the line $\Delta P \gg 4\gamma/D_O$). The tube is electrically conducting (e.g. metallic), and its electric potential ϕ is independently adjusted. This potential polarity is positive, as considered in most experimental studies (to lessen the chance of gaseous discharges). The other electrodes are assumed to be electrically grounded, and located far (many tube radii) away from the drop, so that the

electrical field in the drop region is mostly dependent on the local conditions. The drop will experience a net downward electrical force F_e , of order $\sim \varepsilon_0 \phi^2$, where ε_0 is the electrical permittivity of vacuum (taken as the gas's), a downward gravitational force $\sim F_g \equiv \rho D^3 g$, a downward inertial force caused by the momentum per unit time injected by the flow into the meniscus, $\dot{P} \equiv \rho Q^2 / D_I^2$, and an opposing capillary upward force, expressed as $\sim F_\gamma \equiv \gamma D_O$ when the drop is anchored at the outer edge of the tube. Orientation is important only when the gravitational force on the liquid is relevant. We restrict our discussion to a homogeneous Newtonian fluid, which is characterized by density ρ , dynamic viscosity μ , surface tension coefficient γ , electrical conductivity K , and electrical permittivity ε . The gas phase is assumed to play no role other than act as a dielectric medium with the electrical permittivity of vacuum. Liquid evaporation is not considered here.

The global motions of the liquid meniscus are governed by three dimensionless numbers when we ignore additional effects from viscosity and ohmic conductivity: The Weber number $We_D \equiv \dot{P} / F_\gamma = \rho Q^2 / (D_I^2 D_O \gamma)$, which measures the momentum forces relative to the capillary forces, the electrical Bond number (sometimes called Taylor number; Pantano et al., 1994) $Bo_e \equiv F_e / F_\gamma = \varepsilon_0 \phi^2 / (\gamma D_O)$, which measures the electrical force relative to the capillary force, and the gravitational Bond number $Bo_g \equiv F_g / F_\gamma = \rho D^3 g / (\gamma D_O)$, which compares the gravitational and the capillary forces. Notice that Bo_g does not have a predefined value when setting up an experiment, as it depends on the size of the drop/meniscus (D) that will be formed (and grows with time). Therefore, when comparing experiments another Bond number which depends only on the parameters of the problem is used $Bo_{g0} \equiv \rho D_0^2 g / \gamma$. Ohmic conduction effects can be neglected so long as the characteristic time scale of the meniscus motions, $t_f \equiv D^3 / Q$, is long compared to the liquid electrical relaxation time of the liquid, $t_e \equiv \varepsilon / K$. The relaxation time measures the characteristic time taken by a still conducting body to reach electrostatic equilibrium from a non-equilibrium distribution of charges (Castellanos, 1998). We are also neglecting effects on the meniscus motion due to wetting, such as a moving contact line where the drop is anchored to the tube. Furthermore, the ratio of D_O to D_I is assumed to be close to unity. Accounting for the neglected effects would give additional dimensionless numbers, not considered here.

The next sections are organized as follows: Section 2.2 considers briefly the case when the electrical Bond number is zero or very small. The meniscus motions depend on the Weber and gravitational Bond numbers, with low Weber leading to dripping, while larger Weber (of order unity and exceeding unity) lead to jetting. Section 2.3 considers the case of jetting at Weber of order unity under conditions of large electrical Bond number and small gravitational Bond numbers, $Bo_g \approx 0$. Section 2.4 considers the case of low Weber number, small gravitational Bond numbers, $Bo_g \approx 0$, but electrical Bond numbers up to the electrical Bond number necessary to reach the steady cone-jet (of order unity). These are the conditions leading to the electrohydrodynamic spraying modes, which are also summarized in Table 1. The flow rate Q needed to stabilize steady cone-jet emissions is very small, such that We_D is very small typically. However, the operating Q is not connected to a range of We_D but to another dimensionless quantity to be discussed later in the article.

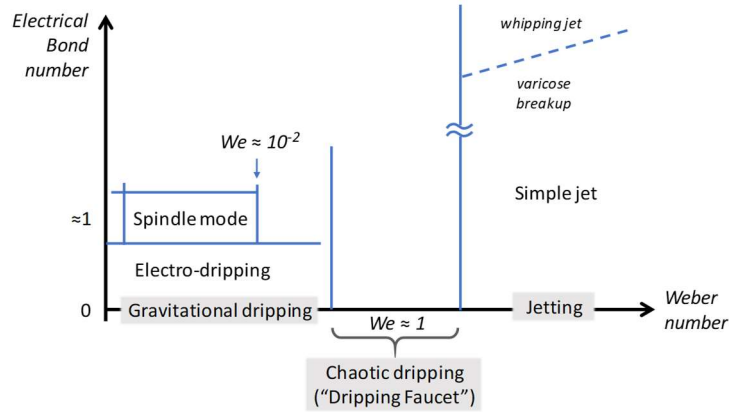


Fig. 2. Schematic map of modes encountered in the (Bo_e, We_D) -plane. The modes in grey boxes are modes for neutral drops ($Bo_e = 0$).

2.2 Neutral and low-charge dripping and jetting ($Bo_e \ll 1$)

We assume that viscous forces are irrelevant. When F_e is insignificant compared to F_γ the sequence of events is like the case of neutral drop. These neutral modes have been reviewed by Clanet & Lasheras (1999) and Eggers & Villermaux (2008). On the (Bo_e, We_D) -plane shown in Fig. 2 these modes lie along the Weber number axis ($Bo_e = 0$). At low enough volumetric flow rate Q , the liquid momentum entering the drop region per unit time can be neglected: $\dot{P} < F_g$. In this mode, the growing drop goes through equilibrium shapes, and eventually falls when the gravitational force $\sim F_g$ (which grows

as the cube of the drop diameter) overcomes the surface tension force $\sim F_\gamma$ (which remains constant), and the process repeats itself. The drop falls when the gravitational Bond number reaches a critical value near unity. This is the *gravitational dripping* mode, on which the drop-weight method for determining the surface tension coefficients of liquids is based.

As the flow rate increases, eventually \dot{P} interferes with the gravitational dripping when the Weber number is no longer small (Clanet & Lasheras, 1999). At a critical value of We_D near unity, the droplet enters a *chaotic dripping* mode, also known as *dripping faucet* (see Fig. 2). At a larger We_D , the motion transitions suddenly to the *jetting* mode, in which a continuous jet is formed, which decays downstream by capillary instability, periodically breaking up into droplets of comparable size, about twice the jet diameter.

For small values of We_D , that is, for gravitational dripping, the effect of a low amount of electrical charge for a perfect liquid conductor is to slightly change the dripping patterns (Notz & Basaran, 1999). As electric potential is raised at constant volumetric rate Q , the frequency of droplet formation increases as the drop volume decreases.

2.3 Jetting at Weber number $We_D \sim 1 - 10$ in the presence of electrical charge

We follow the changes experienced by an initially neutral jet when an electrical potential ϕ is applied to the tube. The liquid-gas interface of the jet becomes charged, due to ohmic conduction through the liquid. The effects due to the surface charge are best classified by using the electrical Bond number Bo_e , introduced above. The jetting and its spray characteristics when the tube was electrified were studied by Marijnissen and co-workers, who referred to this mode globally as *simple-jet* (Agostinho et al. 2012a, 2012b; Ondimu et al. 2017). As ϕ (i.e. Bo_e) increases, the jet does not significantly accelerate in the electrical field, without any major difference in the jet breakup length (Agostinho et al. 2012b). Eventually, at some Bo_e the droplets acquire increasingly more charge and start to form a plume under electrostatic self-repulsion (Agostinho et al. 2012a). Above a critical Bo_e , which grows with the Weber number, the jet undergoes the transition between varicose breakup and whipping jet (dotted line in Fig. 2), leading to a broadening of the droplet size distribution. For water this critical Bo_e increases from 3.8 at $We = (\rho R_j v^2)/\gamma = 4$ to about 6.7 at $We = 17$, where R_j is the radius of the unperturbed jet and

v its velocity, and the electric Bond number is as defined above except it is based on the inner rather than outer diameter (Agostinho et al. 2012a).

2.4. Electro-hydrodynamic modes ($Bo_g \ll 1; We_D \ll 1; Bo_e \sim 1$)

The electrohydrodynamic (EHD) modes are obtained when the Bo_e become of order unity, while the gravitational force and the momentum of the liquid at the tube exit are much smaller than the capillary force: $F_g, \dot{P} \ll F_\gamma$. Therefore, We_D and Bo_g are small. In practice, the effect of Bo_g is flushed by using small tube diameters (using capillary tubes) and voltages high enough so that $F_e \gg F_g$. Under the dominant action of electrical and surface tension forces, the liquid meniscus can adopt a steady conical shape (Taylor cone) if the electrical force is sufficiently high ($Bo_e \sim 1$). If the electrical force is too weak, then the steady shape cannot be sustained and the meniscus pulsates. The main steady and periodic pulsating modes are listed in Table 1. Aperiodic and unstable pulsating modes, as well as steady modes involving corona discharges are not included in Table 1, but are mentioned below. Marginean et al. (2007) said: "Confusing classifications and the lack of consensus on the nomenclature are still major factors undermining the clear understanding of an arguably complex process." Table 1 highlights the main electrohydrodynamic modes with their distinguishing characteristics, as well as alternative terminology used in the literature.

2.4.1. Electrohydrodynamic periodic pulsating modes: Electro-dripping, Intermittent Cone-Jet and Spindle modes

The EHD periodic pulsating modes are the *electro-dripping*, the *spindle*, and the *intermittent cone-jet* modes. These modes are best distinguished using high speed video (Figs. 3 & 4). Electro-dripping refers to the periodic detachment, caused by the electrical force, of one main drop per cycle whose diameter is comparable to the capillary tube diameter. Its domain in Figure 2 is connected to the gravitational dripping line, wherein electrical forces take over gravitational ones as the Bo_e is raised. In contrast, the other two modes occur at Bo_e near unity, with the spindle mode occurring typically at larger Weber numbers (although still $We_D \ll 1$), and the intermittent cone-jet mode at smaller We_D . Experimentally, the intermittent cone-jet and the spindle modes are encountered

from the electro-dripping mode by raising the tube voltage. Bober & Chen (2011) found that it was difficult to consistently obtain single-frequency, single-jet pulsations at voltages exceeding the voltage at which the steady cone-jet was stabilized (at near the minimum flow rate, Q_m in Fig. 3).

In the intermittent cone-jet and the spindle modes, the liquid meniscus develops a cusp during each cycle. In the former, the meniscus evolves through the following stages: development of a conical shape, ejection of a jet, interruption of the jet emission, retraction of the meniscus (Cloupeau & Prunet-Foch, 1990; Marginean et al., 2004; Bober & Chen, 2011; Verdoold et al., 2014). When viewed by the naked eye, the two extreme positions of the interface's oscillation are seen superimposed (Smith, 1986). The jet width varies through the cycle (Marginean et al., 2004; Verdoold et al., 2014), resulting in less monodisperse drops than are possible from steady cone-jets in varicose mode. The intermittent cone-jet mode is usually encountered when electro-spraying conducting fluids, at similar flow rates but slightly lower voltages (thus Bo_e) than are needed to stabilize the steady-cone-jet mode described below. The frequency of oscillation increases as flow rate increases. Bober & Chen (2011) have identified that, within the intermittent cone-jet mode, two regimes can be distinguished: *choked flow* and *oscillating cone* (see Fig. 3). In the choked flow regime, found at lower Q , the jetting frequency f is governed by the supply rate of liquid; therefore, it is linear with Q but does not depend on ϕ . The situation reverses for the oscillating cone regime, in which the jetting frequency becomes independent of Q and dependent on ϕ (see Fig. 3f). In this regime, rises in Q are accommodated by longer duty cycles and thicker jets. Marginean et al. (2007) have described an *astable* mode, which is a chaotic transition between the intermittent cone-jet and the steady cone-jet modes.

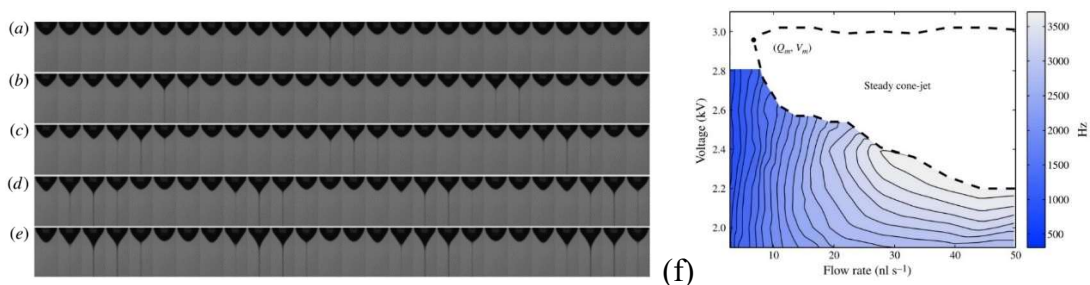
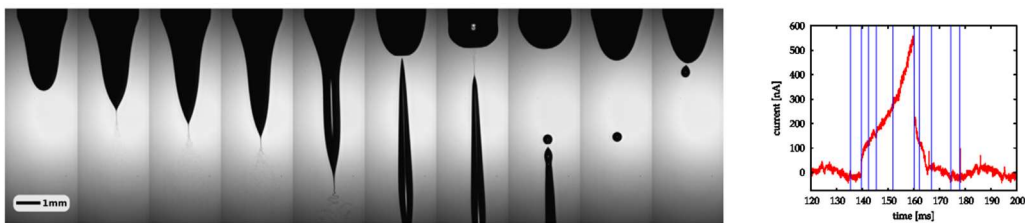


Fig. 3. High speed video frames of a meniscus in the intermittent cone-jet mode as the flow rate increases (a) to (e). (a,b) choked jet regime, (c) transition regime, (d,e) oscillating cone-regime.. Video frame duration is 40 μ s. (f): Frequency contours overlaid on the voltage-flow rate operating diagram. From Bober & Chen (2011).

The spindle mode, typically found at larger We_D (higher flow rates), is characterized by the detachment of one "big" elongated drop (or ligament) per cycle (Fig. 4). Initially in the cycle, the meniscus grows and stretches *while* emitting a cone-jet which ejects fine charged droplets. Meanwhile the ligament grows, and a neck develops at some intermediate position along the ligament, which gets narrower with time, and later pinches off, releasing a spindle-like fragment or drop. This fragment may undergo capillary decay leading to further fragmentation. A backward spraying cone-jet may also form soon after detachment (seventh frame on Fig. 4). The frequency of oscillation decreases as flow rate increases (Hijano et al., 2015). The forward-spraying cone-jet transports negligible mass, but dominant electrical current (Hijano et al., 2015), and can undergo varicose breakup or whipping motions (as shown in Verdoold et al. 2014). Hijano et al. (2015) find the spindle mode to be stable in a wide range of Weber numbers, 10^{-6} and 10^{-2} , but narrow range of Bo_e . At lower than the minimum Bo_e , the system transitioned suddenly to the electro-dripping mode. At higher than the maximum Bo_e , non-axisymmetric meniscus oscillations developed at low flow rates, while, at high flow rates, more than one droplet formed per cycle. Within the stable window of Weber and electrical Bond numbers, two regimes are found depending on the flow rate. For very small Q , the meniscus oscillation frequency (f) non-dimensionalized with the capillary time (t_c), $f' = ft_c = f(\rho D_o^3 / \gamma)^{1/2}$, is of order unity, while at large Q , f' decreases as the inverse of the $1/4^{\text{th}}$ power of the Weber number. Monodisperse droplets of tens of microns could be made at rates of several kHz, for which the charge ratio to the Rayleigh limit was ~ 0.2 (Hijano et al., 2015). In these studies, the slow dynamics of the meniscus are unaffected by ohmic conduction, as the electric relaxation time of the liquid $t_e = \varepsilon/K$ is very small compared to the capillary time t_c .



Config 15, ethanol, 3 mL h^{-1} , Spindle

Fig. 4. High speed video frames of one oscillation in the spindle mode. Liquid is ethanol. $Q = 1.3 \text{ mL/hr}$. Right panel is the measured current trace, and blue straight lines indicate the location in time of each of the video frames. From Verdoold et al. (2014).

The three periodic EHD modes (electro-dripping, intermittent cone-jet, and spindle) have distinct current trace characteristics. In the electro-dripping mode, a single electrical pulse is expected per drop; however, the pulses may be weak and difficult to detect (Verdoold et al., 2014). As voltage is increased, the DC current (averaged over many pulses) increases with steps at the transitions between the electro-dripping, intermittent and steady cone-jet modes. So the transitions between modes can be easily monitored by the DC current. For the spindle mode, the current-time trace is also a periodic succession of nearly identical current pulses, where the current typically varies throughout the pulse (Fig. 4).

2.4.2. Electrohydrodynamic Steady Emission

The steady cone-jet mode is characterized by a conical meniscus (Taylor cone), from whose apex a steady jet emission is formed (Cloupeau & Prunet-Foch, 1989). The conical meniscus need not be strictly a perfect cone, and its shape depends on liquid properties and flow rate. As the electrical conductivity of the liquid is increased, the operational flow rates decrease, and the jet becomes thinner and shorter. At high conductivities for which the jet is short and thin, becoming practically invisible ($K \sim 0.03$ S/m, roughly), the mode can still be identified by the steadiness of the conical meniscus and of the still visible spray, as well as by the fulfilment of the scaling laws of the DC current versus Q and liquid properties (section 3.2.1). At even higher conductivities, both the jet and the spray are invisible.

2.4.3. Cone jet submodes: Varicose breakup and whipping jet

The jet in a cone-jet displays two distinct behaviors (Hartman et al. 2000) (Fig. 5). In the *varicose breakup* submode, the jet is straight and decays by the growth of axisymmetric perturbations (Fig. 5a). The undulations on the jet produce a sequence of swells which grow to periodically form *main droplets*, thus having similar size. Simultaneously, the liquid neck between the swells may lead to the formation of a small droplet, called *satellite*. A bimodal size distribution is therefore common, though truly monomodal distributions are also possible, as demonstrated by Gamero-Castaño (2008).

In the *whipping jet* submode, the jet undergoes lateral motions due to the development and growth of lateral perturbations, the so called *bending instability* (formerly also known

as *kink instability*) (Fig. 5b). Whipping appears when the *growth rate* of lateral perturbations exceeds that of axisymmetric perturbations. In this submode, the jet also undergoes capillary decay into droplets; however, the whipping motion interferes strongly the breakup, resulting in a broadened droplet size distribution (Rosell-Llompart & Fernández de la Mora, 1994). Whipping motions in electrospray are usually chaotic, although a *gentle whipping* submode has been described for heptane (Tang & Gomez, 1996) (Fig. 5c).

The bending instability has also been described for non-Newtonian viscoelastic jets which do not undergo capillary decay (electrospinning). In this case, the jet performs helicoidal motions (Reneker & Yarin, 2008). Helicoidal motions have also been reported in electrified Newtonian viscous liquids discharging into a liquid dielectric medium (Riboux et al., 2011) (Fig. 5f). Helicoidal motions are rare in electrospray, having been observed for water in the presence of a corona discharge (Jaworek & Krupa, 1996; Asano & Yatsuzuka, 1999). Varicose jet and whipping jet submodes are also observed in transient cone-jets, as those found in the spindle and intermittent cone-jet modes (Verdoold et al., 2014) (also Fig. 4).

2.4.4 Additional modes related to corona discharges

In normal air, gaseous electrical discharges appear when electrospraying liquids of high surface tension, typically higher than glycerol, especially water. A way to find out whether gaseous discharges intervene is to carry out the same experiment in gases with different breakdown potentials, e.g. air and CO₂. If the phenomena, especially the electrical current, are the same, then ionization events are not playing a role. Aguirre-de-Carcer & Fernández de la Mora (1995) used this method to show that the steady cone-jet mode of low surface tension liquids does not produce gaseous discharges.

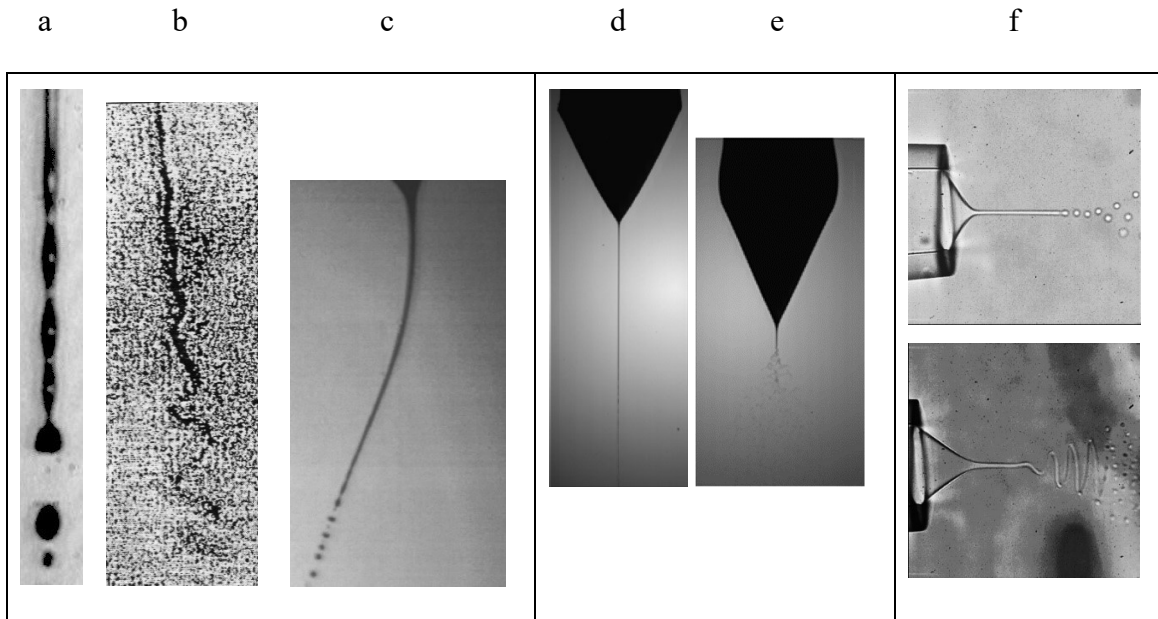


Fig. 5. Jet breakup modes from steady cone-jets: a) varicose wave on heptane jet leads to breakup (jet diameter = $17\ \mu\text{m}$); b) whipping jet (triethylene glycol, LiCl solution, estimated jet diameter $1.5\ \mu\text{m}$); c) gentle-whipping on a heptane jet. Steady cone-jet mode with d) straight jet in varicose breakup mode (ethylene glycol), and e) whipping jet mode (ethanol). Steady cone-jet mode in a liquid-liquid system: Ethylene glycol cone-jet flowing into a bath of 10 cSt silicone oil (tube i.d.= $70\ \mu\text{m}$), with jet undergoing: varicose breakup (top), or helicoidal motions (bottom). Credits: (a) from Tang & Gomez (1994), (b) from Rosell (1994), (c) from Tang & Gomez (1996), (d)-(e) from Verdoold et al., 2014; and (f), courtesy of Alberto Fernandez-Nieves.

On the other hand, Borra et al. (1999, 2004, 2018) have described a high flow rate mode in which water cone-jets are, in fact, stabilized by a continuous glow corona discharge. They name this mode *stable cone-jet glow mode*. Different modes of water menisci in air in the presence of gaseous discharges have also been described by Jaworek & Krupa (1996, 1997, 1999). Tang and Gomez (1995) described a *corona-assisted cone-jet* mode for de-ionized water electrosprayed into a CO_2 atmosphere, using much lower flow rates than in the previous studies. It is possible that this mode was also found by Chen et al. (1995) while electrospraying water-sucrose solutions in CO_2 , which they named *bullet mode*. In both cases, it is not clear whether carbonic acid ions in the water may influence this system. The role of corona discharges in electrospraying has also been discussed by Jaworek et al. (2014). All these studies have made use of relatively wide tubes, a few hundred- μm or more in diameter. López Herrera et al. (2004) showed that when very

narrow tubes are used (diameter $\sim 30 \mu\text{m}$) the steady cone-jet mode occurred in air without corona discharges for deionized water and of dilute HCl/water solutions.

3. The steady cone-jet mode

3.1 Taylor cones, electrohydrostatics

The term "Taylor cone" is used broadly to refer to pointed menisci which form by electrifying the interface between two fluid phases, one of which is electrically insulating (Fig. 1). Conical as well as ogival shapes are included in this definition (Fernández de la Mora, 2007). Taylor cones are found in *steady* cone-jets (Fig. 1a), as well as in *transient* cone-jets, as are found in the spindle mode (Fig. 4), and during the Rayleigh instability of a charged drop (Fig. 1b). Transient Taylor cones are also found when a *neutral* drop is disrupted by a strong electric field (Fig. 1c). In this case, two cones form on either side of the drop. In all these cases, the Taylor cones are accompanied by jet emissions. In the neutral drop case, the emissions from the cones have opposite polarity.

G. I. Taylor, who along with James R. Melcher fathered the field of electrohydrodynamics (EHD) (Melcher & Taylor, 1969; Saville, 1997), showed theoretically that a conical interface can simultaneously satisfy the electrostatic equilibrium (uniform electrostatic potential) and the interfacial mechanical equilibrium (balance of electric and capillary stresses), but only when the cone semi-angle is 49.3° (Taylor, 1964). Experimentally, using water/oil interfaces and soap films, he found that, as the equilibrium shape was approached, the conical menisci became always unstable, emitting a transient jet (Taylor, 1964). Such Taylor cones (without jet) are unstable because, near equilibrium, any tiny bulge on the cone apex region creates an imbalance of electrical force over capillary force, resulting in a net outward pull which causes the bulge to grow even more.

Global stability of the Taylor cone is possible in the steady cone-jet mode thanks to the feedback between electrical field and liquid flow. Under steady state, a perturbation tending to elongate the cone's tip (reducing the cone angle) would momentarily raise the intensity of the electrical field (due to reduced electrostatic shielding). Consequently, the increased electrical stresses would then locally accelerate the liquid flow in this region, where the jet is emitted, prompting a transient reduction in liquid volume, which would restore the original cone angle. A perturbation increasing the cone angle would have the

opposite effect. Higuera (2017) discusses a similar concept involving the stabilizing effect of the charged jet on the Taylor cone.

Another significant difference between the cone of G. I. Taylor and the cones obtained during spraying or during Coulombic events is that these usually have smaller angles than 49.3° . Fernández de la Mora (1992) showed that smaller angles could be predicted after extending Taylor's model to include space charge in the form of a cloud of identical droplet drifting electrophoretically as a conical cloud, resembling an electrospray (Fig. 6a). Experimentally, he reproduced this situation by electro spraying highly conducting liquids ($K \sim 0.03$ S/m), for which the emitted jet is short (of length $L_j \ll L_T$, the height of the Taylor cone) while the spray is still visible (becoming invisible at $K \sim 1$ S/m). As the flow rate Q was raised, the spray cone semi-angle ($\pi - \beta$) increased while the liquid cone semi-angle (α) decreased (see Fig. 6a). In his theory, these two angles are related by a unique function $\alpha = \alpha(\beta)$, where the angles are chosen by the amount of space charge in the spray, set by the ratio $I/(\gamma Z)$, where I is the current, γ the surface tension coefficient, Z the droplet's electrical mobility. In practice, this ratio can be adjusted easily by controlling Q .

This work introduced a notion which influenced subsequent theoretical models: that, at least for high- K liquids, there is an "outer region" defined by the Taylor cone and the spray, and an "inner region" which contains the jet and the transition between the Taylor cone and the jet. The structure of the outer region, at least the Taylor cone, does not depend on the details of the inner jet region. Whereas the inner region is subject to constraints set by the outer region, but not by faraway details like the size and shape of the electrodes (such as liquid feed tube dimensions) or even the applied voltage (Fernández de la Mora, 1992, 2007).

Complementing Taylor's work, Pantano et al. (1994) computed the equilibrium shapes that can form at the end of a cylindrical conducting electrode (tube) depending on applied voltage, in absence of space charge. Equilibrium shapes were found over a finite range of the tube voltage ϕ_0 if meniscus volume and pressure drop were allowed to change (to values which depend on ϕ_0). Fig. 6b shows the predicted menisci for a particular geometry, in which the conical tip of the meniscus was forced to be the Taylor angle. Meniscus shape depends only on the dimensionless voltage or Taylor number defined as $Ta = (\epsilon_0 \phi_0^2)/(2\gamma R)$, where R is the tube's external radius (Fig. 6b). The shapes vary

from ogival at low voltage ($Ta = 3.2$), when the pressure drop is positive, to concave-convex at the highest voltage ($Ta = 14$), where pressure drop was negative. At zero gauge-pressure, the shape was nearly conical ($Ta = 4.66$). Similar trends of shape with applied voltage are commonly observed while operating in the steady cone-jet mode (Fig. 6b, photos).

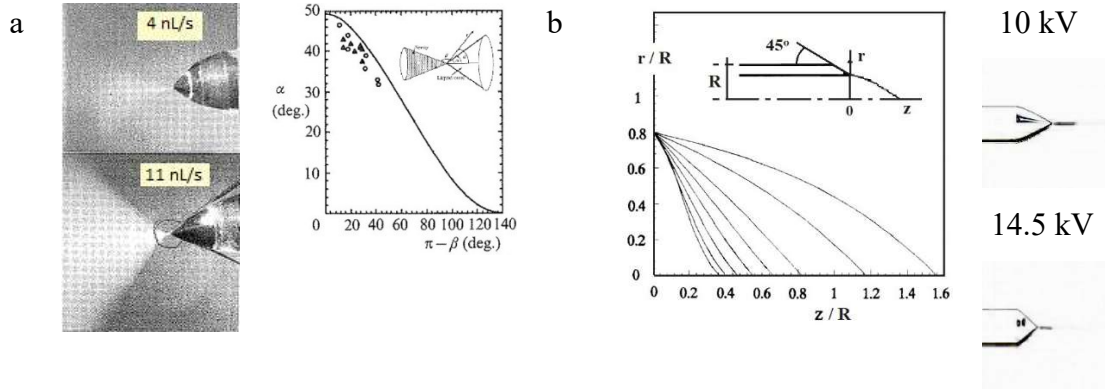


Fig. 6. (a) Electrostatic interaction between Taylor and spray cones for high conductivity liquid, as the total flow rate is increased (left), graph showing liquid cone angle (α) versus spray angle ($\pi - \beta$), experimental data and theory (right) (adapted from Fernández de la Mora, 1992). (b) Equilibrium meniscus shapes as predicted by Pantano et al. (1994) depending on the applied voltage at different Taylor numbers and gauge pressures (adapted from Pantano et al., 1994); and, at right, typical behavior of the Taylor cone as capillary voltage is changed (adapted from Park et al, 2004).

3.2. Jet formation, electrohydrodynamics

3.2.1. Scaling laws

When analyzing the behavior of electrosprays, it is necessary to consider the different scales at which the different phenomena take place. These scales range from the tiny diameter of the jet to the distance between the needle and the collector. The wide disparity of scales and the high number of variables involved (physical properties of the fluid, arrangement and geometrical sizes as well as process variables) have made it difficult to completely understand the mechanisms that control the formation of the electrospray. This has led to controversy about which mechanisms are dominant under different conditions. A difficult region to analyze is where the Taylor cone slims down to begin the formation of a slender jet, the rupture of which will form the drops. A large effort has been devoted to search for the scaling laws that govern this process, i.e., the dimensionless

relationship of variables and their powers that remain approximately constant for some range of electrospray operation.

Fernandez de la Mora et al. (1990) proposed, based on empirical observations, that group $[2\gamma\pi^2r_j^3/(\rho Q^2)]^{1/3}$ is approximately 1 for these systems. In this expression, γ is surface tension, r_j is the radius of the jet, ρ the liquid density and Q the volumetric flow rate. Fernández de la Mora and Loscertales (1994) were the first to propose how the electrical current (I) varies with the volumetric flow rate (Q) after analyzing the phenomenology involved. Based on theoretical considerations, dimensional analysis and their experimental results, they concluded that for liquids with high electrical conductivities (K)

$$I = f(\epsilon_r) \left(\frac{\gamma Q K}{\epsilon_r} \right)^{1/2} \quad (1)$$

where ϵ_r is relative permittivity of the liquid, and f is an empirical function. On the other hand, from pictures of cone-jet systems and considering that the charge relaxation time and flow time should be similar for some value of the jet radius (r_F), they suggested that the jet diameter, D_j , should be of the order

$$r_F = \left(\frac{Q\epsilon_r\epsilon_0}{K} \right)^{1/3} \sim \frac{D_j}{0.4} \quad (2)$$

when $Re = 4\rho Q/(\pi\mu D_j)$ and the dimensionless flow rate $\eta = [\rho K Q/(\gamma\epsilon_r\epsilon_0)]^{1/2}$ are small enough. When these two parameters increase, they suggest that D_j should scale according to the proposal they already presented in 1990, that is to say

$$R_F = \left(\frac{\rho Q^2}{\gamma} \right)^{1/3}. \quad (3)$$

Taking R_F as the radius of the jet, Eq. (3) implies that the kinetic energy of the jet and the surface tension overpressure are similar. These scales were confirmed experimentally by Rosell-Llompart & Fernández de la Mora (1994) with LiCl in tri- and tetra-ethylene glycol solutions. In their experiments, the main droplets' diameters scale with r_F when $\eta \sim 1$ and have a complex dependency with $\Pi_\mu = (\gamma^2\rho\epsilon_r\epsilon_0)^{1/3}/(K^{1/3}\mu)$ as η increases, and asymptotically they tend to scale with R_F .

Gañán-Calvo et al. (1997) also used theoretical considerations, dimensional analysis and experimental results to propose, for liquids with high viscosities and conductivities, for which $[\gamma^3 \varepsilon_0^2 / (\mu^3 K^2 Q)]^{1/3} \ll 1$, the following scaling for the current and the jet diameter

$$I \sim \frac{(\gamma Q K)^{1/2}}{(\varepsilon_r - 1)^{1/4}}; D_j \sim \left[\frac{(\varepsilon_r - 1)^{1/2} Q \varepsilon_0}{K} \right]^{1/3}. \quad (4a,b)$$

When the electrical conductivity and viscosity are low, the relevant scalings were

$$\frac{I}{I_0} \sim \left(\frac{Q}{Q_0} \right)^{1/4}; \frac{D_j}{d'_0} \sim \left(\frac{Q}{Q_0} \right)^{1/2} \quad (5a,b)$$

where $d'_0 = \left(\frac{\gamma \varepsilon_0^2}{\rho K^2} \right)^{1/3}$, $I_0 = \left(\frac{\varepsilon_0}{\rho} \right)^{1/2} \gamma$ and $Q_0 = \frac{\gamma \varepsilon_0}{\rho K}$.

Chen & Pui (1997) considered that for high electrical conductivities, the scaling laws proposed by Fernández de la Mora & Loscertales (1994) and Gañán-Calvo et al. (1997) do not differ significantly, except for their dependence with relative permittivity ε_r . Based on their experimental data ($12.5 \leq \varepsilon_r \leq 182.4$) and considering that the droplets' diameter, D_d , depends on r_F according to

$$D_d = G(\varepsilon_r) r_F \quad (6)$$

they found the following expressions for the functions $f(\varepsilon_r)$ (Eq. (1)) and $G(\varepsilon_r)$

$$f(\varepsilon_r) = -449 - 0.21\varepsilon_r + 157\varepsilon_r^{1/6} + 336\varepsilon_r^{-1/6} \quad (7a)$$

$$G(\varepsilon_r) = 10.87\varepsilon_r^{-6/5} + 4.08\varepsilon_r^{-1/3}. \quad (7b)$$

Gañán-Calvo (1997) developed an electrohydrodynamic model from which they derived another scaling law for liquids whose electrical charges are relaxed fast enough compared to the hydrodynamic movement:

$$I = 4.25 \left[\frac{Q K \gamma}{\ln\left(\frac{Q}{Q_0}\right)^{1/2}} \right]^{1/2}; r_G = Q^{1/2} \left(\frac{\rho \varepsilon_0}{\pi^4 \gamma K} \right)^{1/6} \sim \frac{D_d}{2.3}. \quad (8a,8b)$$

In their analysis, neither I nor D_d turned out to depend on relative permittivity, over the wide range $1.9 \leq \varepsilon_r \leq 111$. He argued that fluids with high polarity typically exhibit high conductivities and consequently high Q/Q_0 experimental values. This coincidence may have been taken as a dependency with ε_r , when it is, in fact, a dependence with $\ln(Q/Q_0)$.

From a one-dimensional model that describes the acceleration process when Taylor's cone slims down to form the jet, Hartman et al. (1999a) found

$$I \sim (\gamma K Q)^{1/2} \quad (9)$$

where the non-dependency with ε_r agrees with Gañán-Calvo (1997). However, their experimental results do not confirm the dependency of I on $\ln(Q/Q_0)^{1/2}$. On the other hand, they also found that D_d has a dependence with K and Q closer to those found by Gañán-Calvo (1997).

Independently, Gañán-Calvo (1999) modified his previously proposed scaling law valid for high volumetric flow rates compared to Q_0 , to propose, based on a quasi-one-dimensional model of the cone-jet system and experimental results,

$$\frac{I}{I_0} = k_I \left(\frac{Q}{Q_0}\right)^{1/2} ; \quad \frac{D_d}{d_0} = k_D \left(\frac{Q}{Q_0}\right)^{1/2} \quad (10a,b)$$

which are valid at much lower flow rate, and where $k_I = 2.6$ and $k_D = 2.9$ are experimentally adjusted constants. Except for the value of k_D , the expression for D_d is the same he found in 1997.

Hartman et al. (2000) investigated the jet breakup mechanism, both experimentally with a high-definition digital camera, as well as with a mechanistic model of the development of the disturbances which lead to the jet breakage. This model predicts $D_d \sim Q^{1/2}$. Experimentally they found that for low conductivity liquids jet breakup occurred in varicose mode and $D_d \sim Q^{0.48}$, confirming their model and Gañán-Calvo (1999)'s prediction. Under conditions of high electric current, their jets developed whipping motions before breaking up into droplets, for which according to their model and experiments $D_d \sim Q^{1/3}$.

Ku & Kim (2002) studied experimentally the size of electrospray drops produced from high viscosity liquids (of the order of 1000 cP), and found that $D_d \sim Q^{1/3}$, although the drop size was between 2 to 6 times larger than predicted by previous scaling laws.

Gamero-Castaño & Hruby (2002) measured the characteristics of the drops emitted in a vacuum-operated cone-jet. When comparing how the radius of the jet at breakup varies with the r_F and r_G scalings (Eqs. (2) and (8b)), they found that their results could not discern which of the two scales were the most appropriate. This results from the facts that

r_F/r_G depends on small powers of Q and K and that r_F and r_G refer to the radius at the location where the jet is formed, which is different from the value at the breakup point, located downstream. They also argue that, owing to viscosity effects in the formation of droplets from jets with moderate or high conductivity ($K \geq 10^{-3}$ S/m) and/or high viscosity, the ratio between the main droplet diameter and that of the jet is not 1.89 (Rayleigh's value), as often taken, but higher (around 2.6 in their experiments).

Higuera (2003) formulated the equations governing the electrohydrodynamics in the transition region between the cone and the jet (Fig. 7a). The solutions of the equations were governed by the three dimensionless parameters Q_0 , ε_r and $(\rho\varepsilon_0\gamma^2/K)^{1/3}/\mu$, and they showed that at high flow rates $I \sim Q^{1/2}$, independent of ε_r .

Gañan-Calvo (2004) identified different scalings for the current and jet diameter, from asymptotic analyses of the terms in the slender approximation of the liquid momentum balance equation for the cone-to-jet transition zone. Six scalings were found when each of the three predominant hydrodynamic forces (inertia, surface tension, viscous forces) are combined with the electrostatic force predominating in the cone-necking region (polarization, suction). When inertia and electrostatic suction dominate

$$I \sim (\gamma K Q)^{1/2}; D_j \sim \left(\frac{\rho \varepsilon_0 Q^3}{\gamma K} \right)^{1/6}. \quad (11a,b)$$

These scalings are valid when

$$\alpha_\rho \gg \alpha_\mu^{1/4}; \frac{\alpha_\rho}{\varepsilon_r - 1} \gg 1 \quad (12a,b)$$

where $\alpha_\rho = \frac{\rho K Q}{\gamma \varepsilon_0}$; $\alpha_\mu = \frac{K^2 \mu^3 Q}{\varepsilon_0^2 \gamma^3}$.

If inertia and polarization forces dominate, then

$$I \sim \left[\frac{\rho K^2 Q^2}{(\varepsilon_r - 1) \varepsilon_0} \right]^{1/2}; D_j \sim \left(\frac{\rho \varepsilon_0 Q^3}{\gamma K} \right)^{1/6} \quad (13a,b)$$

which is applicable when

$$1 \gg \frac{\alpha_\rho}{\varepsilon_r - 1} \gg \frac{\alpha_\mu}{(\varepsilon_r - 1)^4}. \quad (14)$$

And when the viscous forces and the electrostatic suction dominate,

$$I \sim (\gamma K Q)^{1/2}; D_j \sim \left(\frac{\mu \varepsilon_0^2 Q^3}{\gamma K^2} \right)^{1/8} \quad (15a,b)$$

applicable when

$$\alpha_\rho \ll \alpha_\mu^{1/4}; \frac{\alpha_\mu}{(\varepsilon_r - 1)^4} \gg 1. \quad (16a,b)$$

This regime is also found in electrospinning. Additionally, the author provided scaling laws when viscous and polarization forces dominate, and two others in which surface tension dominates, but could not be checked against experimental data.

Higuera & Barrero (2005) did an order-of-magnitude analysis considering a relatively long jet of a highly polar liquid ($\varepsilon_r \gg 1$) (which may not always be realized experimentally), and found two scaling relationships depending on the flow rate level, both independent of liquid viscosity. For high rate, $I \sim Q^{1/2}$, and for low rate,

$$\frac{I}{I_0} \sim \frac{Q/Q_0}{\varepsilon_r^{1/2}} \quad (17)$$

Smith et al. (2006) showed that the power n in the relationship $I \propto Q^n$ depends experimentally on the molar conductivity Λ_m (S cm²/mol) for various solutions, as

$$n = 0.051 \ln(\Lambda_m) + 0.410 \quad (18)$$

over the range $1.2 \leq \Lambda_m \leq 214$ S cm²/mol; therefore, $0.42 \leq n \leq 0.68$.

Basak et al. (2007) in an experimental study where they made particles of iron oxide, predicted the dependence of the particle diameter D_p with flow rate Q in Eq.(2), provided the variation of conductivity K with precursor concentration C was taken into account, as

$$D_p \sim \left(\frac{QC}{K} \right)^{1/3}. \quad (19)$$

Gañán-Calvo & Montanero (2009) noted that, when properly scaled, the physics of electrospray and of flow focusing cone-jet systems obey the same scaling laws. They found that for a large amount of published data $D_d/2 \sim r_G$ at low flow rates, when $We = \rho Q^2 / (\pi^2 r_G^3 \gamma) < 20$ (compatible with Rayleigh jet breakup).

Higuera (2009) analyzed the equations governing the meniscus region of an electrospray of a very polar liquid to investigate the scaling $I(Q)$. Between a minimum flow rate and $Q/Q_0 \approx 1$, the electric current scaled as $I/I_0 \sim [Q/(\varepsilon_r Q_0)]^{1/2}$; while between $Q/Q_0 \approx 1$ and $Q/Q_0 \approx \varepsilon_r$, $I/I_0 \sim Q/(\varepsilon_r^{1/2} Q_0)$; and, finally, when $Q/Q_0 > \varepsilon_r$, $I/I_0 \sim (Q/Q_0)^{1/2}$.

Maißer et al. (2013) determined by nDMA the diameters of salt clusters in the sub 10 nm size range after neutralizing electrospray droplets generated from high conductivity and permittivity aqueous solutions. The dependence of the dimensionless particle diameter with the dimensionless volumetric flow rate was compared with the scaling laws $D_d \sim Q^{1/3}$ and $D_d \sim Q^{1/2}$, claiming that the results agreed with the latter under the assumption that some of the gas phase ions produced for neutralization were incorporated into the droplets.

Gañán-Calvo et al. (2013) proposed scaling laws for the minimum flow rate Q_m which maintains the structure of a cone-jet. These laws come when considering the symmetries derived from the time invariance under steady state. They compared these laws against experimental data available in the literature and distinguished two regimes when the flow rate approaches Q_m : (i) when viscous force and (ii) when the polarization force destabilize the cone-jet. Case (i) occurs when $\varepsilon_r \delta_\mu < 1$ where $\delta_\mu = [\gamma^2 \rho \varepsilon_0 / (\mu^3 K)]^{1/3}$ (electrohydrodynamic Reynolds number) and then Q_m scales with Q_0 / δ_μ . In case (ii) $\varepsilon_r \delta_\mu > 1$ and Q_m scales as $\varepsilon_r Q_0$.

However, Scheideler & Chen (2014) experimentally determined Q_m for fluids of different viscosity, and observed that while $Q_m \sim Q_0$ for slightly viscous liquids, when viscosity increases the diameter of the tube on which the cone is anchored, D_b , becomes relevant and then $Q_m \sim \gamma D_b^2 / \mu$.

Wang et al. (2017) conducted a visualization study with a high-speed camera on the different modes of operation of ethanol electrosprays using a double nozzle system. In the cone-jet mode, the diameter of the generated droplet follows the scaling given by Eq. (10b), with $k_D = 0.65 \pm 27\%$, 4.5 times smaller than the value found by Gañán-Calvo (1999).

Park et al. (2017) performed a series of experiments to identify the different stable operating regimes for water in air at atmospheric pressure from a narrow non-metallic capillary. In the cone-jet mode, the diameter of the drops obtained followed the scaling given by Eq. (6) with $G(\varepsilon_r) = 0.88$, which agrees with the findings of Loscertales & Fernández de la Mora (1995) also for water. In addition, when plotting $(D_d/R_F)2^{1/3}$ in front of the volumetric flow rate, they obtain a decreasing curve that asymptotically tends to ~ 0.5 , as found by Rosell-Llompart & Fernández de la Mora (1994).

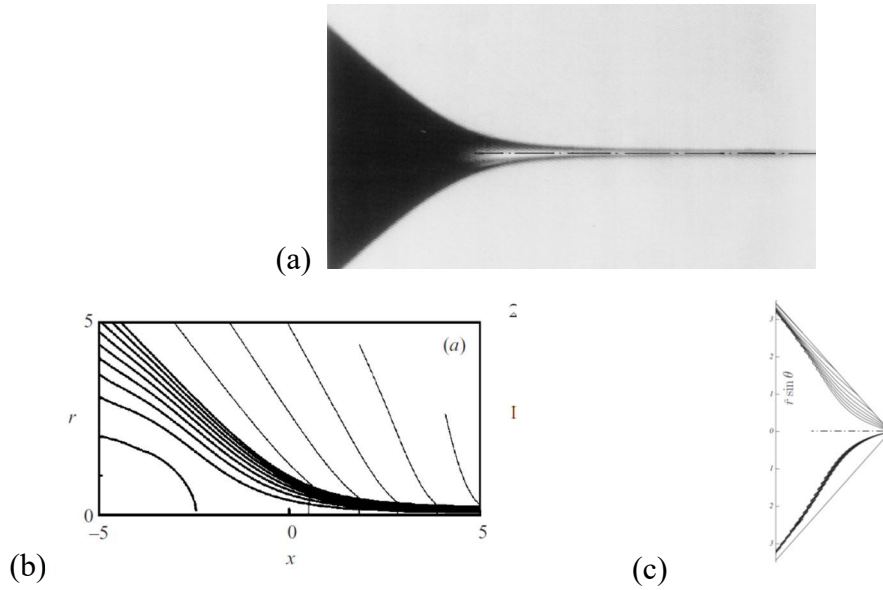


Fig. 7. Structure of the transition region: (a) Picture adapted from Gañán-Calvo (1997); (b) Streamlines and the electric equipotential lines for $\epsilon_r = 5$, $Re = 1$ and $Q/Q_0 = 0.27$, from Higuera (2003). (c) Equispaced iso-contours for positive electric charge density (upper half) and negative electric charge density (lower half) in a Taylor cone (adapted from Higuera, 2009).

3.2.2. Detailed modeling of the transition region

Apart of the scaling laws, one can describe the relationships between relevant variables through establishing mathematical models of the principles that govern the main mechanisms, and then solve the resulting equations. The laws needed to model the transition region include: i) the electrostatic forces governed by Coulomb's law, ii) mass conservation, iii) charge conservation, and iv) momentum conservation. These laws are complemented with specific conditions fulfilled at the gas-liquid interface, such as the surface charge as a function of the inner and outer electrical field components normal to the interface, and the balances of normal and tangential forces acting on the interface. Since the cone-jet system presents very different length scales, the problem is very *stiff*, which makes the set of governing equations difficult to solve. Therefore, in most of the studies, the size of the cone-to-jet transition region is assumed small compared with any other length of the system.

As presented in the previous subsection, Gañán-Calvo (1997) extended Taylor's electrostatic solution for the static conical meniscus to include an infinitely long and thin emitted jet. He postulated that, even when the liquid is a *leaky dielectric* (Saville, 1997),

in liquid flow time scales much longer than the electrical relaxation time ($\epsilon_r \epsilon_0 / K$), the charges are found only on the liquid surface, and the internal electric field is negligible compared to the external field. Under this hypothesis, he obtained Eqs. (8a) and (8b).

A model with additional elements in the system, like a tube and a flat counter-electrode, was presented by Hartman et al. (1999b). They used the slender jet approximation for the entire cone and jet, and solved the resulting set of equations numerically in an iterative manner. The numerical solution of the transition region outline agreed with the experimental one. They estimated that space charge has a 5-7% influence on the electrical field strength on the cone surface.

The slender jet approximation cannot consider the existence of internal circulation in the cone. Such circulation was photographically demonstrated by Hayati et al. (1987) and by Barrero et al. (1998, 1999). These authors showed that liquids with large electrical conductivity and viscosity (low Reynolds numbers) favor the formation of meridional circulation (toroidal patterns in the cone), while low electrical conductivity with low viscosity (high Reynolds) induce helicoidal trajectories.

Cherney (1999a,b) laid out the equations of electro-hydrodynamics, and applied them to the cone, and to the jet in the slender approximation. He solved the problem by perturbation methods at low flow rates. His results were consistent with Eq. (1), the function $f(\epsilon_r)$ was closer to Chen & Pui's (1997) proposal when considering either the change in effective surface tension by surface charges (Cherney, 1999a) or the dilatant viscosity on the surface (Cherney, 1999b).

Higuera (2003) numerically solved the equations governing the system in the transition zone *without* using the slender jet approximation. His solutions depend only on three dimensionless parameters: the dimensionless flow rate Q/Q_0 , the relative electrical permittivity ϵ_r and the Reynolds number $Re = \left(\frac{\rho \epsilon_0 \gamma^2}{\mu^3 K} \right)^{1/3}$. In the cone, he found the internal circulation described by Barrero et al. (1998, 1999) (see innermost streamline in Fig. 7b). At large Q/Q_0 the electrical current was dominated by conduction within the liquid and the surface of the cone was nearly equipotential. In this asymptotic regime, the electrical current increases as $Q^{1/2}$ and is independent of the dielectric constant.

The behavior of an electrospray made with a very small meniscus was analyzed by Higuera (2004) using both order of magnitude estimates and numerical solutions of the

model. He obtained the order of magnitude of different system parameters, such as the position where the electrical transport by conduction ceases, the jet radius, and the electrical current versus the volumetric flow rate, depending on how the power $-n$, of decay of the electric field strength with axial distance. The case $n = 0$ corresponds to a meniscus emerging on one of two parallel electrodes. $n = 1/2$ is the case of a large Taylor cone, for which the Taylor solution dominates the electrostatic field. And $n = 1$ is the case of a cone emerging from a cylindrical tube. He found $I \sim Q^{\frac{4-5n}{5-4n}}$; therefore, only when $n = 1/2$, the electrical current scales as $I \sim Q^{1/2}$.

Considering that the meniscus is shaped like a Taylor cone, Higuera (2009) analyzed the flux and the distribution of charge for the case of very polar dilute solutions of strong electrolytes, using a detailed model of the electro-hydrodynamic problem in the limiting case of a *sink flow*. Figure 7c shows, for a positive electric current, an example distribution of the charge density near the apex showing an outer positive charge layer and an inner negative one. At some small flow rate there is complete charge separation and negative charges do not reach the apex, whereas no steady state solutions could be found for smaller flow rates. Such minimum flowrate is of the same order as the experimentally determined minimum flow rate for electrosprays of highly polar, low viscosity liquids.

Carretero & Martínez-Sánchez (2004) laid out the conservation equations in spherical coordinates in a unidimensional approximation of the Navier-Stokes equations, including conservation of mass, conservation of charge, and boundary conditions for the normal and tangential stresses at the surface. The relationship between current and flow rate obtained from the solutions reproduce that found by Fernández de la Mora & Loscertales (1994), including the shape and values of the function $f(\varepsilon_r)$.

3.2.3. CFD studies

The development of versatile commercial software for *computational fluid dynamics* (CFD) has encouraged its use for simulating cone-jet systems for given values of the governing parameters. A challenge for this approach is to describe the cone-jet flows at vastly different length scales. Therefore, most studies have considered either narrow tubes or low conductivity liquids, producing thick jets. From the available simulations, it is still difficult to extract general tendencies or order of magnitude relationships.

Lastow & Balachandran (2006) used the software CFX 4.4 for simulating the dynamics of formation of cone-jets for heptane and ethanol. The method of *volume of fraction* (VoF) was used to compute the position of the liquid-gas interface. In this study, they solved the momentum transport equation including the Coulombic force due to the electrical charges in the liquid, and the electrical fields inside and outside of the liquid. Their model is made of balances between electrostatic and hydrodynamic forces, and does not address electrical current. Their results, including the stability ranges of the cone-jet mode, and droplet diameter versus the liquid flow rate, were consistent with experimental data from the literature.

Almost simultaneously, Sen et al. (2006) studied the case of an electrospray in which the liquid supply tube is dielectric, and contains a carbon fiber inside to help stabilize the formation of the cone-jet. For their simulations, they used the software FLOW3D and they validated favorably their model comparing their numerical simulation results with the experimental results by Hartman et al. (1999a). They attribute a difference of 5 to 10% between the simulated and the experimental electrical current values, to their neglect of the space charge generated by the electrospray (as did Hartman et al. (1999a)). Once this effect is considered, their predictions are reconciled with experiments. As a follow up on this work, Sen et al. (2011) included the breakup of the jet to form droplets. In order to validate the model, they simulate the breakup of a system like the experimental one reported by Hartman et al. (2000). The velocity and diameter of the droplets were consistent with the experimental results with about 10% discrepancies.

To simulate numerically an *Array of Micromachined UltraSonic Electrosprays* (AMUSE) (ion source for mass spectrometry), in which the droplet formation and its charge were determined by separate processes, Forbes et al. (2010) adapted a commercial code (FLUENT v6.3) to solve the electrohydrodynamic equations. To validate their model, they simulated two kinds of cone-jet systems: one with finite electrical conductivity, and another in which the liquid is a perfect conductor. The results compared well, at least qualitatively, with experimental observations.

Lim et al. (2011) developed a model which included continuity and Navier-Stokes equations for the liquid and for the gas phases, as well as the volumetric stresses caused by the electrical charges (polarization and Coulombic stresses), plus Poisson's equation to compute the electrical potential. They performed experiments using dichloromethane (DCM), as solvent with low electrical conductivity and permittivity, thus large

characteristic electrical relaxation time (of a few milliseconds). Since this characteristic time is not negligible compared to the characteristic time scale of viscous flow, the *leaky dielectric model* for the charge transport is not applicable. The electrical charge distribution at the liquid-gas interface was selected from fitting the shape and size of the cone and the jet to experiments. Their simulations covered different length scales, ranging from the inter-electrode separation (cm scale) to the cone-jet system and the droplets formed. The measured droplet size and the one obtained from the simulations were reasonably close.

Xu et al. (2013) used the same model, and the commercial code FLUENT to simulate the structure of the cone-jet, and the jet breakup into droplets for the case of a tube with two coaxial channels, which is configured for producing composite core-shell microspheres (see section 4), again, using DCM as solvent. The absence of a reliable model for the electro-hydrodynamics of this liquid was now addressed by adjusting the surface electric charge computed using Gauss's law by a factor, until computed and experimental meniscus profiles agreed. Figure 8 shows the system and the equipotential lines from the needle to the droplets, and the flow field, revealing two toroidal vortices in the cone. Their simulations overestimated the sizes of the microspheres compared to the experimental results. Yan et al. (2016) expanded the model to include the possibility of miscibility between the two coaxial liquids, and solved the equations using FLUENT. They conclude that it is possible to obtain stable Taylor cones with this geometry and miscible liquids, while it becomes harder to attain stability when the liquids are immiscible and display a high liquid-liquid interfacial tension. They also found that particle sizes were dependent on the geometry of the ends of the channels.

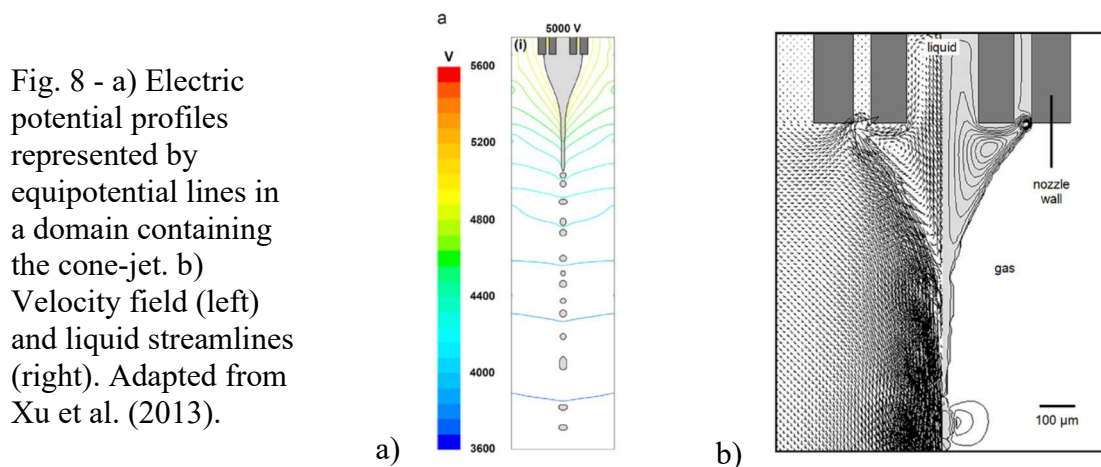


Fig. 8 - a) Electric potential profiles represented by equipotential lines in a domain containing the cone-jet. b) Velocity field (left) and liquid streamlines (right). Adapted from Xu et al. (2013).

Sarkar et al. (2013) studied the formation of Taylor cones and ensuing jet using the commercial software ConventorWare, in a system whose dimensions were much smaller than typical real systems to reduce computational resources. The profiles of the liquid-air interface in the simulation agreed with the experimental ones, after normalizing by the tube radius.

Wei et al. (2013) used OpenFOAM to simulate the formation of the cone, its continuation into a jet, and its breakup to form droplets, for a low conductivity liquid (heptane), for which they obtained jets whose diameter is of order 10% that of the tube. They found (i) that both the droplet diameter and the electric current depend on applied voltage, (ii) that the cone length and the jet diameter increase with applied voltage (in agreement with experiments), and (iii) a dependence of jet length on applied voltage, against experimental observation.

Dastourani et al. (2018) developed a mathematical model of the cone-jet plus the surrounding air system, and solved the resulting equations with OpenFOAM for heptane. The mean droplet diameters obtained by simulations agreed with the experimental ones obtained by Tang & Gomez (1996). The liquid flow pattern showed the presence of vortices close to the emitter exit. The size and position of the vortices were strongly dependent on liquid flow rate and moderately dependent on applied voltage.

3.2.4. Physics summary

We consider here the simplest case of a dissolved strong electrolyte, and consider a conducting needle which is set at a positive potential. The negative ions travel towards the needle, wherein electrochemical reaction takes place, releasing electrons to the needle. The circulation of these electrons through the electrical system constitutes the electrical circuit current which feeds the high potential to the needle. The positive part of this current (positive ions) is transported towards the jet, both by conduction through the liquid bulk (I_b) as by convection on the liquid-gas interface (I_s). Since we assume steady state and axisymmetry (around the z -axis), the electrical current crossing any cross-section to the z -axis must be constant and be the sum of the two contributions (Melcher & Warren, 1971; Gañán-Calvo, 1997; Higuera, 2003):

$$I = I_b + I_s = 2\pi K \int_0^R E_z^i r dr + 2\pi R v_{sz} \sigma \quad (20)$$

where E_z^i is the axial component of the electrical field inside the liquid, $R = R(z)$ is the radial position of the cone-jet interface, v_{sz} is the z-component of the liquid velocity on the interface and σ is the surface electric charge density. A transfer between charge conduction and convection takes place due to the presence of a finite internal electrical field \mathbf{E}^i , whose normal component at the interface (E_n^i) feeds the surface electrical charge by ohmic conduction. Therefore,

$$\frac{dI_s}{dz} = -\frac{dI_b}{dz} = 2\pi R K E_n^i \left[1 + \left(\frac{dR}{dz} \right)^2 \right]^{1/2}. \quad (21)$$

The external electrical field \mathbf{E}^o becomes shielded in the bulk of the liquid due to the presence of the surface electrical charge, which according to Gauss's law satisfies:

$$\sigma = \varepsilon_0 (E_n^o - \varepsilon_r E_n^i). \quad (22)$$

Under the hypothesis of zero free charge in the surrounding gas medium and inside the liquid, the electrical potential in each phase fulfills Laplace's equation ($\nabla^2 \varphi^o = 0$; $\nabla^2 \varphi^i = 0$). These equations, once solved, provide the electrical field vectors ($\mathbf{E}^o = -\nabla \varphi^o$; $\mathbf{E}^i = -\nabla \varphi^i$).

The liquid movement, supposedly in laminar regime, is governed by the Navier-Stokes equation:

$$\rho \mathbf{v} \cdot \nabla \mathbf{v} = -\nabla p + \nabla \cdot (\boldsymbol{\tau}^\mu + \boldsymbol{\tau}^e) + \rho \mathbf{g} \quad (23)$$

where the divergence of the viscous stresses tensor is $\nabla \cdot \boldsymbol{\tau}^\mu = \mu \nabla^2 \mathbf{v}$, and that of the Maxwell electrical stress tensor is $\nabla \cdot \boldsymbol{\tau}^e = \rho_q^i \mathbf{E}^i - \frac{1}{2} (E^i)^2 \varepsilon_0 \nabla \varepsilon_r + \frac{1}{2} \varepsilon_0 \nabla \left[(E^i)^2 \rho \frac{\partial \varepsilon_r}{\partial \rho} \right]$ (Landau & Lifshitz, 1984; Saville, 1997). In these equations, μ is the dynamic viscosity coefficient, ρ_q^i is the electrical bulk charge density in the liquid, ρ is the liquid mass density, and \mathbf{g} the gravitational acceleration vector (only relevant in the description of large cones). Inside the liquid, the three terms of the divergence of the electrical stress tensor are usually negligible. The first one is so because the concentration of charge in the liquid is small (usually considered zero); the second and third because the relative permittivity is assumed to be homogeneous within the liquid, and the liquid is incompressible.

As for any flow field, in addition, the equation of continuity must be satisfied, which for an incompressible fluid is $\nabla \cdot \mathbf{v} = 0$. At the interface, several conditions must be fulfilled for the normal and tangential stresses. Normal stresses must cancel (Higuera, 2003), so

$$p = \gamma \nabla \cdot \mathbf{n} + \mathbf{n} \cdot \boldsymbol{\tau}^\mu \cdot \mathbf{n} - \mathbf{n} \cdot \boldsymbol{\tau}^e \cdot \mathbf{n} \quad (24)$$

where p is the effective pressure, inside of the liquid (its pressure inside minus that at the gas phase), γ is the surface tension coefficient, \mathbf{n} is a unit vector normal to the liquid-gas interface pointing to the gas phase, and $\mathbf{n} \cdot \boldsymbol{\tau}^e \cdot \mathbf{n} = \tau_n^e$ is the normal electrical stress at the interface, which is given by (Saville, 1997)

$$\tau_n^e = \frac{1}{2} \varepsilon_0 \left[(E_n^o)^2 - \varepsilon_r (E_n^i)^2 \right] + \frac{1}{2} \varepsilon_0 (\varepsilon_r - 1) E_t^2. \quad (25)$$

The first term on the right-hand side of the Eq. (24) gives the capillary contribution; the second one the viscous stresses at the surface, and the last one the electrical normal stresses due to the presence of electrical charges on the surface. In Eq. (25), E_t is the tangential component of the electrical field on the liquid surface, which is the same inside as outside of the liquid (to satisfy the second equation of electrostatics, that the rotational of the electrostatic field is zero).

The viscous and electrical tangential stresses at the interface must balance, therefore,

$$\mathbf{t} \cdot \boldsymbol{\tau}^\mu \cdot \mathbf{n} = \sigma E_t. \quad (26)$$

Finally, under steady state the restriction to forbid liquid motion in the normal direction of the interface is

$$\mathbf{v} \cdot \mathbf{n} = 0 \quad (27)$$

As the liquid moves through the Taylor cone, net charge builds up on the interface, supplied by ohmic conduction from the liquid bulk. The capillary (surface tension) stress must balance this increasing normal electrical stress, and the only possible way to do so, is to reduce the meniscus radius (as the surface tension stress varies as γ/R). While electrical conduction is what maintains the electrical current inside the liquid meniscus (Taylor cone), at its apex it is surface convection of charge at the interface. There, the liquid is no longer shielded electrically and the tangential electrical stress drives the liquid motion. Such electrical stress transfers momentum to the interior of the jet by means of the liquid viscosity. As the jet moves forward, it becomes convectively unstable, in the sense that small perturbations of its surface, at certain wave numbers, have a tendency to

grow. Such amplification results in the breaking of the liquid column of the jet, releasing the droplets whose diameter is proportional to the jet diameter. Such droplets, driven by the initial inertia and the electrical field, move forward, and spread developing the electrospray.

3.3. Spray plume structure

Virtually all applications of electrospray are dependent on how the droplets distribute themselves within the spray plume. This is evidently true for film formation and coating (Jaworek, 2007b), electrospray ionization mass spectrometry (Fenn, 2003; Barrios-Collado, et al., 2016), and colloidal thrusters (Gamero-Castaño, 2008; Tang et al., 2011).

3.3.1. Experimental results on spray structure

Experimental methods

The main experimental techniques used for studying electrospray plumes include: (i) optical imaging of the spray plume under continuous illumination (taken e.g. using a photo camera with a macro lens), (ii) droplets imaging with a microscope by pulsed shadowgraphy (flash photography in bright field illumination) or high-speed video (Hartman et al., 2000), and (iii) phase Doppler anemometry (PDA) for locally getting droplet size and speed information (Tang & Gomez, 1994). PDA is based on droplets crossing a small volume defined by the intersection of two coherent Gaussian laser beams, the “control volume” or “probe volume” PV. Each droplet crossing the PV sends oscillatory light pulses or "bursts" into two or more photodetectors, which are later deconvoluted to extract the droplet speed (from the burst frequency), and the droplet size (from the pulses' phase shift). By accumulating signals from many droplets, the *local* joint distribution of droplet size and one component of the droplet velocity are obtained. PDA is capable of sensing at high rates (e.g. 10^4 droplets \cdot s $^{-1}$), and covers a wide range of droplet diameters, from ~ 0.2 to $300\ \mu\text{m}$ (Naqwi 1994). Therefore, this technique is adequate to probe the structure of electrosprays, or just to determine droplet size (Snarski & Dunn, 1991; Gomez & Tang, 1991; Dunn & Snarski, 1992; Dunn et al., 1994; Gañán-Calvo et al., 1994; Naqwi, 1994; Tang & Gomez, 1994; Grace & Dunn, 1996; Naqwi et al., 1996; Olumee et al., 1998; Hartman et al., 1999b; Wilhelm et al., 2005; Wilhelm &

Mädler, 2006; Wortmann et al., 2007). Two-color PDA allows the simultaneous determination of two droplet velocity components, but has been used rarely (Nemes et al., 2007).

PDA requires the presence of a single particle in the probe volume. Therefore, the PV cannot be located very near the jet. The maximum number density n_{max} in Tang and Gomez (1994) with a heptane electrospray at $D_m = 32 \mu\text{m}$ was $3 \times 10^{10}/\text{m}^3$, which was attained at ~ 4 mm from the jet breakup point. It was $5 \times 10^9/\text{m}^3$ in Hartman et al. (1999b) with a $D_m = 18 \mu\text{m}$ ethylene glycol spray measured from 7 to 26 mm below the jet. In Gañán Calvo et al. (1994) $D_m = 50 \mu\text{m}$, at $z = 12$ mm from tip of needle (Expnt. #1). For electrosprays, the number density increases rapidly as the droplet size decreases. Therefore, the PV must be even further from the jet to avoid droplet coincidence.

In the jet region, sizing droplets with diameter above about $10 \mu\text{m}$ is possible by pulsed shadowgraphy (Tang & Gomez, 1994). However, this technique has not been used with smaller droplets because their shadows are less well defined. To deal with invisible sprays in vacuum Gamero-Castaño (2008) obtained maps of electrical current density by scanning a detector across the spray.

Results on the varicose mode: satellite formation

A well-known feature of electrosprays formed in varicose jet breakup mode (section 2.4.3) is the formation of a faint halo under continuous illumination (Fig. 9a). Such halo is an outer spray cloud, made of only satellite droplets, which surrounds an inner spray plume, made of main droplets. In this mode, the jet releases droplets approximately in a line, but small displacements out of perfect alignment are quickly magnified by the transverse component of the electrostatic field, which increases as the droplet gets further from the jet axis (Tang & Gomez, 1994; Hartman et al., 1999b). The transverse force is similar for satellite or primary droplets under the same theoretical displacement, but the satellite droplets, being smaller, accelerate faster and attain larger radial velocities. (Note that droplet mass, not electrical mobility or specific charge, is the critical factor.) In addition, a droplet-free or “dark” zone is often left between the two spray clouds (Tang & Gomez, 1994; Wilhelm & Mädler, 2006) (see Fig. 9a,b). In the case of very small satellite droplets (e.g. $D_s < 0.5 \mu\text{m}$), it may be difficult to appreciate the satellite shroud. Invisible droplets outside the main plume could be detected by spatially resolved current measurement (as applied by Tang & Gomez, 1994, with visible sprays).

Size segregation was studied initially by John Zeleny (1917), and more proof of its mechanism was presented in the studies by Tang & Gomez (1994) and Hartman et al., (1999b) for sprays with D_m of 32 and 18 μm , respectively. In these studies, flash photography of the jet breakup and the PDA methodology were combined. Satellite segregation has also been reported in electrospray beams in vacuum (Gamero-Castaño, 2008), with D_m between 0.56 to 1.13 μm .

Satellite droplets formed by varicose breakup may be absent from the spray zone if they merge with the primary droplets during the jet breaks up process. This “satellite merging” phenomenon has been long known for non-electrostatic sprays (Eggers, 1997), but has only been discussed in a handful of electrospray works (Cloupeau & Prunet-Foch, 1989; Hartman et al., 2000; Gamero-Castaño, 2008).

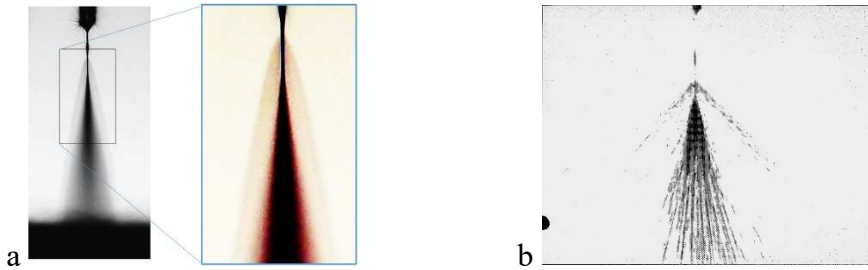


Fig. 9. Size segregation of satellite droplets in electrosprays. (a, b): Examples of satellite segregation under darkfield illumination (images shown are negative converted): (a) for ethylene glycol with NaCl ($K=3.3 \times 10^{-4}$ S/m) at $Q = 3.7 \mu\text{l}/\text{min}$, $I=78$ nA, in parallel plate capacitor configuration; flash exposure photograph under continuous illumination (courtesy of Nikolas Sochorakis); (b) Close up of breakup region under 25 ns flash illumination for heptane with 0.3%wt Stadis 450, $Q = 167 \mu\text{L}/\text{min}$, $D_p=32 \mu\text{m}$, $D_s=10 \mu\text{m}$ (adapted from Fig. 3 of Tang & Gomez 1994).

Results on the varicose mode: main droplets

The plume of main droplets opens gradually as they move away from the jet breakup region (e.g. Fernández de la Mora, 1992; Gamero-Castaño, 2008). In addition, the *main* droplets segregate radially by size. This is especially noticeable if the droplets' size dispersion is "large", e.g. 20% RMS as in the PDA and numerical study by Gañán-Calvo et al. (1994). Similar “monodisperse” and “polydisperse” sprays showed that the droplet *axial* speed decreased in the *radial* direction. This is expected because the electrical field

lines spread out from the centerline. However, this decrease (radial gradient) was greater in the polydisperse case, because, away from the centerline, the smaller droplets are relatively more abundant than in the monodisperse case, as they move slower. As the smaller droplet size fractions migrate away from the centerline the local mean droplet size increases along the axis (Fig. 10a).

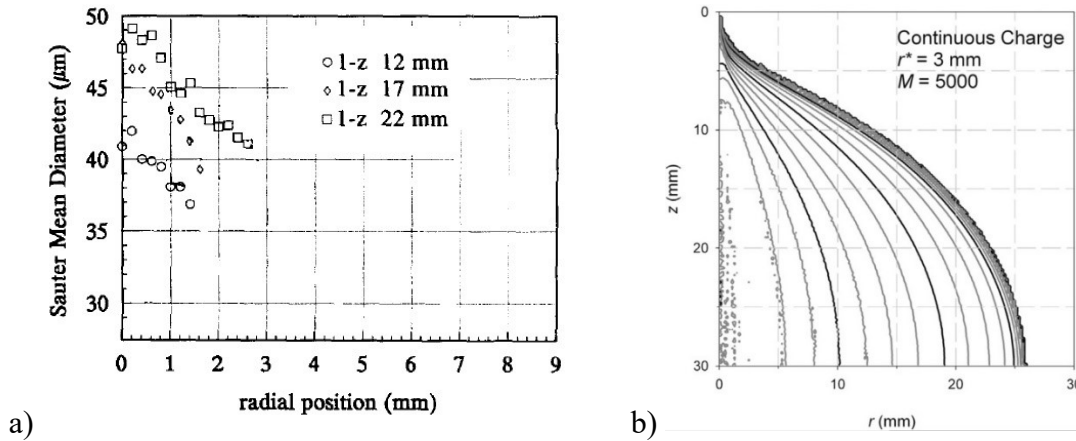


Fig. 10. The size of main droplets in polydisperse electrospays increases along the spray axis, due to the migration of smaller droplets away from the axis. (a): Droplet size PDA data versus radial position at three distances from the needle tip (shown in the legend) for droplet size RSD $\sim 20\%$ (heptane 0.6%vol Stadis 450, $Q = 138 \mu\text{L}/\text{min}$, $I = 43 \text{ nA}$) (adapted from Fig. 7a of Gañán-Calvo et al., 1994). (b): (z,r)-map of droplet diameter from a Lagrangian simulation for the same RSD but smaller droplet diameter, count mean diameter of $8.84 \mu\text{m}$ (Grifoll & Rosell-Llompart, 2014).

Tang & Gomez (1994) combined PDA and flash photography data with balance equations to gain insights into the physics of electrospays. They characterized by PDA the structure of a (nonvolatile) bimodal heptane cone-jet electrospay in varicose jet breakup mode producing main droplets $32 \mu\text{m}$ in diameter. By entering the PDA data into the spray momentum equation, they determined the electrical field along the spray axis. Along the spray axis, the electrical field and the main droplet number density decayed precipitously. The droplet axial speed decayed much slower than the electrical force, due to the substantial initial droplet inertia, decaying ultimately under the action of the drag force. The droplet axial velocity attained the maximum value at the axis. On the other hand, the number density (surprisingly) had a local minimum at the spray axis, becoming maximum at a finite radial distance from the axis (at all axial positions). They also determined that

the electrical charge distribution was narrow (relative standard deviation of 0.15) by balancing droplet drag and electrical force far from the needle where the droplets were in electrophoretic motion. The axial component of the electric field was found to be mostly that due to the electrodes (external field), while the radial component of the electrical field was found to be mostly the repulsive field due to the spray droplets. One should note that sprays of much smaller droplets may behave differently.

3.3.2. Numerical spray modelling

All the above effects have been predicted in numerical simulations of electrosprays, providing additional detailed information on these phenomena, e.g. for the region near breakup. The numerical approaches can be classified in two wide groups: (i) the Eulerian models, which predict the droplet number density as a continuous function of space and time, by integration of mass and momentum conservation equations, plus Gauss' law for the electric potential (Poisson's equation) (Higuera, 2012), and (ii) the Lagrangian models, in which the individual trajectories of all the droplets in the spray are solved in 3D space using Newton's equation of motion (Gañán-Calvo et al., 1994).

3.3.2.1. Droplet dynamics

Lagrangian models seek a solution of the equations of motion of the droplets in 3D, which describe the variation in time t of position vector \mathbf{R}_i (of the droplet center) and velocity \mathbf{U}_i for each droplet i :

$$\frac{d \mathbf{R}_i}{dt} = \mathbf{U}_i ; m_i \frac{d \mathbf{U}_i}{dt} = \sum_{\mathbf{k}} \mathbf{F}_{\mathbf{k},i}. \quad (28a,b)$$

Eq. (28b) expresses Newton's second law, stating that the droplet's mass m_i times its acceleration equals the sum of different forces exerted on the droplet (summation over index k). The relevant forces are the drag force $\mathbf{F}_{\text{drag},i}$ (zero if the spray is in a vacuum) and the electrical force $\mathbf{F}_{\text{electrical},i}$; whereas added mass, Basset, gravitational and Brownian motion forces can be neglected (Crowe et al., 1998). Therefore,

$$m_i \frac{d \mathbf{U}_i}{dt} = \mathbf{F}_{\text{drag},i} + \mathbf{F}_{\text{electrical},i}. \quad (29)$$

Brownian effects on droplet's dynamics in electrosprays are negligible, even for nano-sized droplets (so long as their electrical charge is a significant fraction of the Rayleigh

limit charge q_R , and the electrical field does not drop to negligible values).

In Eq. (29), the electrical force experienced by droplet i is the product of the droplet's charge q_i times the electrical field at the location of the droplet $\mathbf{E}(\mathbf{R}_i)$, that is, the field which would be at the droplet location if the droplet were removed from the system without displacing any other charge, including the electrodes'. This force is usually decomposed as

$$\mathbf{F}_{\text{electrical},i} = q_i \mathbf{E} = \mathbf{F}_{\text{external},i} + \mathbf{F}_{\text{space-charge},i} + \mathbf{F}_{\text{induced},i}. \quad (30a)$$

The first summand is the force due to the electrodes potential differences, assuming there were no other droplets in the system:

$$\mathbf{F}_{\text{external},i} = q_i \mathbf{E}_{\text{ext}}(\mathbf{R}_i) \quad (30b)$$

wherein the "external field" $\mathbf{E}_{\text{ext}}(\mathbf{R}_i) = -\nabla\phi_e$ can be viewed as a driving field. It is computed, once for the entire simulation, by solving Laplace's equation for the part of the electrostatic potential due to the electrodes $\nabla^2\phi_e = 0$, usually extending the spraying needle with an equipotential Taylor cone. The second summand in Eq. (30a) gathers the Coulomb repulsion force due to all the other droplets considered as point-like charges j ($\neq i$):

$$\mathbf{F}_{\text{space-charge},i} = q_i \mathbf{E}_{\text{sp}}(\mathbf{R}_i) = \frac{q_i}{4\pi\epsilon} \sum_{j \neq i}^N q_j \frac{\mathbf{R}_{ij}}{R_{ij}^3}. \quad (30c)$$

Here \mathbf{R}_{ij} is the displacement between the position vectors of droplets j and i , $\mathbf{R}_{ij} = \mathbf{R}_i - \mathbf{R}_j$, and ϵ is the electrical permittivity of the gas. Finally, the third summand in Eq. (30a) is a small correction accounting for the attraction to the induced charges on the electrodes surfaces (image charges) by the presence of spray charges. Many Lagrangian simulations of electrosprays have considered the capillary-to-planar collector configuration, where only the force due to charges induced on the collection plate is taken into account, using the "image charge" approximation, as:

$$\mathbf{F}_{\text{induced},i} \approx \mathbf{F}_{\text{images},i} = -\frac{q_i}{4\pi\epsilon} \sum_j^N q_j \frac{\mathbf{R}_{ij}}{R_{ij}^3} \quad (30d)$$

where \mathbf{R}_{ij} is a vector joining the i charge with the "image charge" of droplet j . This "image force" accelerates the droplets very near the collection plate, increasing the impaction speed of the droplets. To be efficient, Eqs. (30c) and (30d) are usually computed together in the code.

The drag force on droplet i moving through a medium (here, gas) of density ρ_g and viscosity μ_g is expressed through a drag coefficient C_{Di} such that:

$$\mathbf{F}_{\text{drag},i} = \frac{\pi}{8} D_i^2 \rho_g |\mathbf{U}_g - \mathbf{U}_i| (\mathbf{U}_g - \mathbf{U}_i) C_{Di} \quad (31)$$

where \mathbf{U}_g is the local velocity vector of the gas phase in the neighborhood of the droplet. C_{Di} is taken usually for an isolated *solid* sphere moving through uniform gas flow, and is a function of the Reynolds number $Re_i = \rho_g |\mathbf{U}_g - \mathbf{U}_i| D_i / \mu_g$ (Clift et al., 1978). The isolated solid sphere function for C_{Di} may break down in the jet breakup region.

Along the droplet trajectory, droplet inertia (LHS term of Eq. 29) is important near the jet breakup region, where the electrical field varies rapidly with distance. Inertia weakens while the rate of change of the field decreases, at a time scale which is large compared to the droplet relaxation time τ (Hinds, 1999), i.e. the characteristic time for a droplet to attain a new steady motion after a change in hydrodynamic conditions. Eventually, droplets and gas are in dynamic equilibrium, i.e. $\mathbf{F}_{\text{drag},i} \approx -\mathbf{F}_{\text{electrical},i}$: the droplet motion becomes *electrophoretic*. If, in addition, Re_i is small enough, the drag is linear with velocity and the droplet velocity becomes $\mathbf{U}_i \approx \mathbf{U}_g + Z_i \mathbf{E}$, where Z_i is the electrical mobility of droplet i . In sum, electrophoretic motion is achieved downstream from the jet beyond a distance $l \gtrsim U_{jet} \tau$. One visual proof of this is that the angle at which the droplet trajectories (including the outline of the spray) meet a conducting collector at 90° . When it does not, the collector may be experiencing electrical potential variations over its surface (as noted by Bodnár & Rosell-Llompart, 2013, due to electric charge buildup on polymeric particulate coatings).

3.3.2.2. Lagrangian models' implementation and the "N-squared problem"

In a Lagrangian computation, the system time t progresses in steps, and the droplets are introduced sequentially in the computational domain. The droplets's size and charge are picked randomly from a joint droplet size and charge distribution function $f(D, q)$. However, this predefined function is usually assumed to be "thin" around a curve $q(D)$, in agreement with experimental findings by de Juan & Fernández de la Mora (1997). Therefore, droplets are picked from a probability density function $g(D)$, which is experimentally determined (Hartman et al., 1999b; Grifoll & Rosell-Llompart, 2012), or it is defined from the experimental moments (e.g. as a lognormal in Gañán-Calvo et al.,

1994; Grifoll & Rosell-Llompart, 2012). Then, the charge $q(D)$ is usually computed either by assuming constant droplet volumetric charge density (charge over volume) or as a constant fraction of the Rayleigh limit charge $q(D) = D^{3/2}$.

The droplet's initial velocity is taken as axial, equal to jet's, in a consistent manner, e.g. from either experiments or scaling laws. This velocity is computed typically considering the volumetric flow rate and the jet diameter, which is obtained from the droplet diameter and the linear theory of breakup of neutral jets ($D_d = 1.89 D_j$). The droplet's initial axial position has been taken either as randomized within a range (Gañán-Calvo et al., 1994) or has been defined by the droplet volume centroid (Grifoll & Rosell-Llompart, 2012). The initial radial position is chosen randomly from a spatial distribution usually Gaussian in radius and isotropic in azimuth (Gañán-Calvo et al., 1994; Grifoll & Rosell-Llompart, 2012). Hartman et al. (1999b) find that a width of this distribution below one jet radius does not significantly impact the spray structure.

Due to the lengthy computations involved, *explicit* integration schemes of the equations are often used, such as the Euler method (Gañán-Calvo et al., 1994) or the Ermak method (Grifoll and Rosell-Llompart, 2012). An explicit scheme uses the position and velocity of a droplet at time t to predict the next values at time $t + \Delta t$. However, explicit methods require short time steps Δt , of order $1\ \mu\text{s}$ (Grifoll & Rosell-Llompart, 2012).

N-squared problem

A key aspect of Lagrangian computations is the substantial number of droplet-droplet interactions that must be computed at each time step (Eq. (30c)). Their number scales as $N(N - 1)/2 \approx N^2$, where N is the number of droplets in the system (or "spray droplets"), which can easily be in the order of 10^5 or more. CPU computational time (CPU time) has been significantly reduced by simplifying the computations of Eqs. (30c) and (30d). The "coarse-graining" strategy used by Grifoll & Rosell-Llompart (2012) subdivides the spray (and the "image spray" inside the collector) into cells, whose charges within are replaced by a "lumped charge". Forces are then computed droplet-by-droplet only for neighboring droplets (i.e. those in the same cell or in neighboring cells), while the force due to more distant droplets is based on the cells' lumped charges. Additional CPU time is saved by integrating using different time steps in different zones of the spray. Grifoll & Rosell-Llompart (2014) have explored finding the electrical field $\mathbf{E}(\mathbf{R})$ as a solution to Poisson's

equation for the electrostatic potential. This "continuous droplets' charge" method considers the droplets charge as a continuum, except those in regions where the nearest neighbor interactions between droplets is dominant, i.e. near the jet breakup and the spray centerline (for the simulated case of a polydisperse spray). They found that solving Poisson's equation is computationally costlier than the addition of the pair-wise repulsion forces (in 30c and 30d), but its solution needs only be updated once every many (~ 1000) time steps. Since the electrodes are included, this takes care of the induced-charge part of the force (most of it). On a spray with $N = 2.6 \times 10^4$ the coarse-graining strategy method reduced the CPU time by a factor of 39 with respect to the full computation, while the continuous droplet's charge method reduced it by a factor of 112. The efficiency of these methods increases as N gets larger, expected if the liquid's electrical conductivity K is increased, resulting in smaller droplets.

Higuera and coworkers have proposed the use of the "Particle-In-Cell" method in which each "particle" represents a constant number of droplets, having the same size and moving with the same speed (Higuera, 2016a, 2016b; Higuera and Tejera, 2017). This methodology is valid when the inter-droplet distance is much greater than the droplet radius, and the spray is monodisperse or bidisperse, so droplets' close encounters can be neglected. (When the spray is polydisperse differences in electrophoretic droplet velocity along the axis causes "collisions"; Grifoll & Rosell-Llompart, 2014.) The problematic jet breakup region is excluded by considering an extractor plate orifice, at which the outgoing droplets fluxes are specified as inputs. In addition, they have applied Poisson's equation to find \mathbf{E} .

The above approaches have not yet been adapted to deal with systems with millions of interacting droplets, as are encountered in densely packed multiplexed electrospray sources (MES) (except for the infinite array case, for which periodicity conditions apply Higuera, 2016a). Yang et al. (2012) have demonstrated the potential of Graphics Processing Units (GPUs) for simulating such systems (see also Lojewski et al., 2013). A known "failure mode" of MES, is the path reversal of satellite droplets, and consequent liquid accumulation on the extractor plate. To be able to predict the minimum field strength necessary to prevent path reversal, Deng and Gomez (2007) proposed a "line-of-charge" approximation. The model is based on replacing the space charge field ($\mathbf{E}_{sp}(\mathbf{R}_i)$ in Eq. (30c)) by the field created by a line of uniform charge density (charge per unit length equal to the electrical current over jet velocity). This model was validated for a

single electro spray against a Lagrangian model of the spray (Fig. 11). Although not accurate inside of the main-droplets plume, the model can predict accurately its outline, as well as the satellite droplets' spray shroud.

In conclusion, Lagrangian simulations have focused on electro sprays with main droplet size in the several micro-meters to several tens of micrometers range ($> 5 \mu\text{m}$), because at these sizes the number of droplets per spray is still manageable (of order 10^4 - 10^5). As more efficient software and/or hardware strategies are implemented to address the N-squared problem, Lagrangian models should become powerful tools for the detailed numerical description of much finer sprays. Another need in the field is the quantification of the prediction accuracy of any numerical strategies by comparing to experimental data. Detailed data sets against which models can be validated/compared exist only for large ($D_m > 10 \mu\text{m}$) droplet sizes obtained by PDA systems (see section 3.3.1). For example, models have been validated against PDA data include $D_m = 32 \mu\text{m}$ in Arumugham-Achari et al. (2013) and $10 \mu\text{m}$ in Yang et al. (2012). Therefore, as the capability to handle fast simulation methods advances, a need arises to develop experimental methods and data sets describing the structure of electro sprays made of much finer droplets.

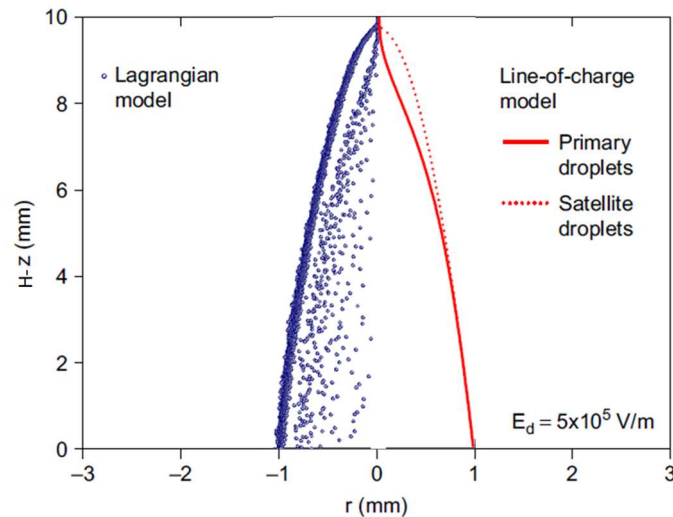


Fig. 11. “Uniform line-of-charge” model validated against Lagrangian model for an individual electro spray (adapted from Deng and Gomez, 2007). Extractor plate is at $H-z = 10 \text{ mm}$. Main droplet mean diameter $\sim 10 \mu\text{m}$.

3.3.2.3. Eulerian models

The simplest Eulerian models apply to dilute sprays of monodisperse droplets. The droplet number density is assumed to be a continuous function of position and time, and it is computed by integration of the mass and momentum conservation equations, and Gauss' law for the electric potential (satisfying Poisson's equation) (Higuera, 2012, 2013). Polydispersivity could be accounted for by each class of the size distribution histogram as a separate "aerosol species" whose number density is governed by its own mass and momentum conservation equations. Poisson's equation would then be solved by considering the charge density contributed by all size classes.

Eulerian models are more difficult to implement when the aerosol is not dilute. In a dilute system, the electrostatic interactions between droplets can be computed from the local average of the electric field generated by both the droplets and the external electrodes. However, close enough to the droplet generation zone the spray is not dilute. This region is characterized by high droplets' number density and speed, and strong electrostatic droplet-to-droplet interactions (Grifoll & Rosell-Llompart, 2012). In such a region, an Eulerian model would require the inclusion of a collision term from extensive information about the statistics of these collisions, which usually is not available (Higuera, 2012).

3.3.2.4. Numerical predictions on spray structure

One of the first successes of Lagrangian models were their ability to predict size segregation for the main droplets (Gañán-Calvo et al., 1994), as well as of satellite droplets (Hartman et al., 1999b) (Figs. 10b, 12a). Additionally, numerical simulations studies have allowed predicting the contribution to the electrical field by the space charge, which has been elusive (Tang & Gomez, 1994). Fig. 13 shows that space charge contributes strongly, both axially and radially, to the electrical potential (thus to its gradient, \mathbf{E}). The contribution to the field by the space charge is to significantly increase the radial field component, increase the axial component near the collector, and decrease the axial field at the jet breakup region. Note that "space charge" includes images in the collector plate (Eq. (30d)).

Another interesting fact is that the satellite droplets in the spray can greatly outnumber the main droplets, despite having comparable production rates (Arumugham-Achari et al. 2013). Therefore, the space charge due to satellite droplets may not be negligible.

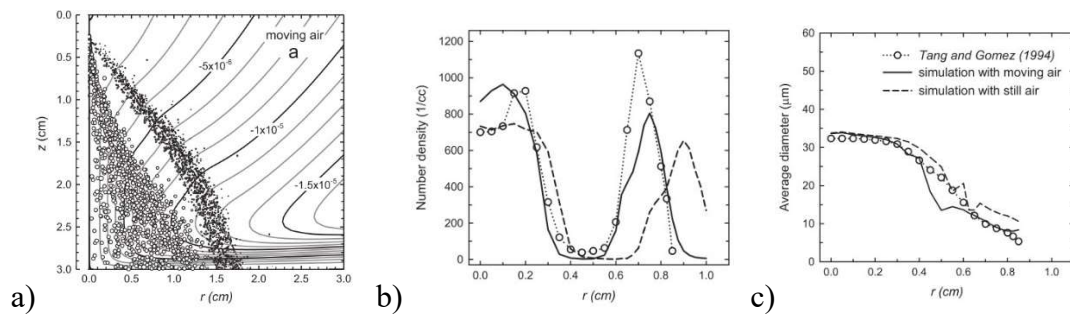


Fig. 12- Numerical simulation with induced gas flow by Arumugham-Achari et al. (2013) for an electrospay characterized by PDA by Tang & Gomez (1994). (a): Snapshot displaying droplet z - and r -positions and streamlines of the induced air flow. (b,c): Comparison of experimental data (circles) and predicted radial profiles at $z = 1.2$ cm of (b) droplet number density, and of (c) droplet diameter. The needle tip is at $z=0$, while the flat collector is at $z=3$ cm. Note that the trajectories do not arrive at 90° because the droplet motion is not in the electrophoretic regime (inertia being important).

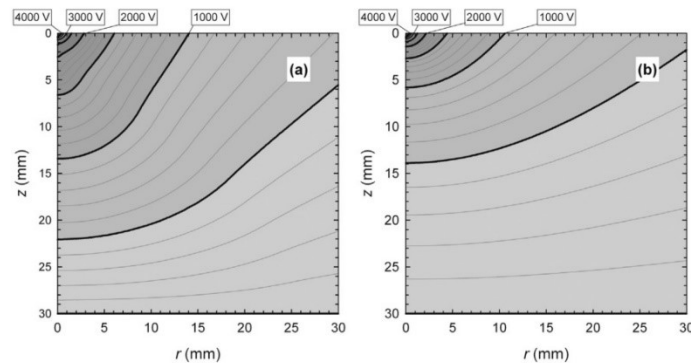


Fig.13. Electric iso-potential lines for the external field (right) and in the presence of a spray of main droplets (left). Adapted from Grifoll & Rosell-Llompart (2014).

Furthermore, the gas flow motion induced by the reactive drag force exerted by the droplets on the gas has been quantified. Hartman et al. (1999b) concluded that the axial velocity of the gas phase induced by the droplets' drag (not included in their model) must be relevant. The induced gas motion (sometimes called "entrainment") had been previously neglected in many studies, based on estimates which say that, globally, droplets cannot cause significant gas motion. On the other hand, Arumugham-Achari et al. (2013) defined a framework in which the gas steady state momentum equation includes a source term due to the droplets' motion. For the case of the bimodal electrospay

experimentally studied by Tang & Gomez (1994), they found that including the induced gas motion improved the predictions of droplet number density, velocity, and local size distribution (Fig. 12). When a gas flow is imposed (forced flow), it could be trivially included by introducing a position dependent gas velocity field in Eq. (31), so long as it significantly exceeds the induced flow.

Going forward, the collection flux data predicted by Lagrangian models (Oh et al., 2008; Jung et al., 2010) could be fed as input to film growth models (Rodríguez-Pérez et al., 2005) or pattern formation using masks, either dielectric masks (Morozov & Morozova, 1999; Wei et al., 2013), or electrostatic focusing masks for high resolution patterning (Kim et al., 2006; You & Choi, 2007; Lee et al., 2009). Another area of use of Lagrangian models is droplet neutralization or discharging by counterions to prevent Coulombic explosions (Higuera, 2016b).

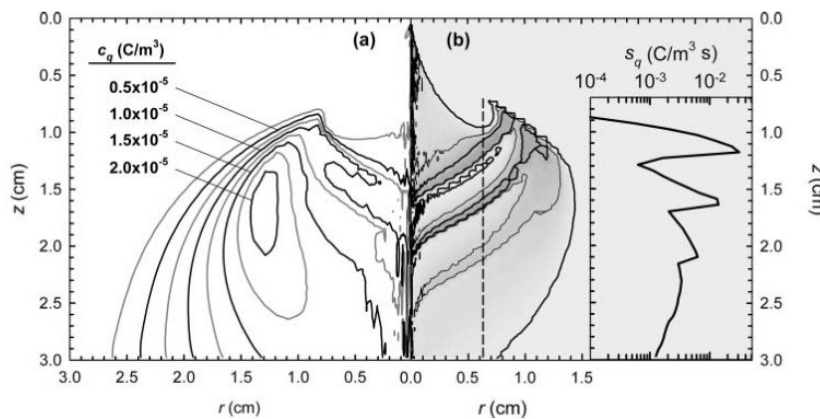


Fig. 14. Contour maps corresponding to an evaporating methanol electro spray under induced gas motion, of (a) residual charge concentration, and (b) volumetric rate of generation of residual-charge, which reveals fringes corresponding to the first three Rayleigh instability events of the droplets. Inset: values along the dashed line. From Arumugham- Achari et al. (2015).

3.3.2.5. Volatile electro sprays

The evaporation of electro spray droplets must be controlled in electro spray ionization mass spectrometry (Barrios-Collado et al., 2016), and in film formation and coating by electro spray deposition (Jaworek, 2007b). In electro spray ionization, ions are transferred to vacuum after being produced in an electro spray at atmospheric pressure. In this process, ions are transferred from solution to the gas phase by field-desorption from very

small droplets which are obtained only after significant solvent evaporation and subdivision by Coulomb explosions in the spray. In film formation by pyrolysis, a suitable precursor dissolved in the electrospray droplets decomposes onto a heated collector to form a coating. As noted by Wilhelm et al. (2003) for yttria-stabilized zirconia films, the quality of the film depends on the solvent content of the impacting droplets, and can be degraded by the presence of submicron particles produced during Coulombic explosions. Predicting the state (diameter, composition, temperature) of the droplets in the spray requires droplet evaporation models. Simple diffusive evaporation models (Hinds, 1999) have been used in some works. However, when Re , the Reynolds number for the droplets's motion relative to the air, is large enough the Sherwood number should be corrected (Rietveld et al, 2006) using evaporation *convective* models (e.g. the Abramzon–Sirignano, 1989; Miller et al., 1998). In addition, the computation of the evaporation rates in the entire spray also requires the solvent vapor concentration and temperature fields in the gas phase, in addition to the gas velocity flow field. To simplify the computation, some studies have considered stagnant gas conditions, and impose solvent vapor background concentration and gas temperature fields, e.g. zero or fixed solvent vapor concentration (Wilhelm et al., 2003; Rietveld et al., 2006; Sen et al., 2011), and e.g. gas temperature profiles experimentally determined without the droplets' presence (Wilhelm et al., 2003; Wilhelm & Mädler, 2006).

One way to include all effects is the fully-coupled framework of Arumugham-Achhari et al. (2015), which comprises a Lagrangian droplet model, a convective droplet evaporation model, and Eulerian codes for the gas flow (in this case, induced) and the transport in the gas phase of solvent vapor, heat, and dry residues. One interesting prediction of this work is the location of the droplet Coulombic explosion events, which occurred in conical bands within the spray (Fig. 14b). Transport of solvent vapor and heat in the gas phase was predominantly convective at macroscopic scales. Vapor concentration was high enough to be relevant only near the droplet generation region, where the droplets spend little time. Higuera (2016a) and Higuera & Tejera (2017) have presented a similar model, and extended it with the combustion of the solvent vapor, relevant for electrosprays injected into microcombustors (Kaiser et al., 2003; Kyritsis et al., 2004).

Evaporative electrospray models could be expanded to include other relevant phenomena, such as solvent fractionation when the droplets contain multiple solvents (Kiselev et al. 1997; Zhou & Cook 2000); solute transport within the droplet, combined with chemical

reactions and phase transitions, which are necessary for predicting particle morphologies; and nanoparticle agglomerate formation within droplets of electrosprayed colloids (Hogan & Biswas, 2009).

4. Extension to multi-fluids: coaxial and parallel flows

Modified versions of standard EHD spraying involves issuing more than one fluid simultaneously. Among those, there have been reports in which liquid emulsions have been electro-atomized, but other embodiment resort to more complex nozzles through which two or more fluids flow independently to form a compound meniscus upon which the electric forces are applied to, eventually, atomize the compound meniscus into compound droplets. Perhaps the more familiar embodiment is the so-called coaxial or compound electrospray reported by Loscertales et al. (2003). In this one, two immiscible fluids flow at their own flow rates through a nozzle consisting of two concentric capillary tubes (needles), such that one fluid flows through the inner needle, the *core fluid*, while the other flows through the gap between the inner and the outer needle, the *sheath fluid* or *shell fluid*. This configuration allows forming a compound meniscus at the nozzle tip, which deforms into a coaxial Taylor cone when an appropriate electric voltage difference is applied between the nozzle and some nearby electrode. A highly-charged compound or coaxial jet ensues from the tip of the compound Taylor cone, with the core liquid surrounding the sheath one, which breaks up into core-shell droplets. Although Chen et al. (2000) where perhaps the first reporting the use of a coaxial needle, in their case the liquids used where miscible, and the aim of the setup was to stabilize the Taylor cone of the mixed fluids at the tip of the coaxial needle. Figure 15 shows two pictures of compound Taylor cone-jets. Although other nozzles with parallel channels (Mou et al., 2012) or with more than two coaxial tubes have been reported (Kim & Kim, 2010; Lee et al. 2011; Cao et al. 2014a, 2014b; Zhang et al., 2017; Chen et al., 2018), we shall focus here on the two tubes coaxial nozzle. We must also mention that this coaxial configuration has been broadly used since the past decade to form core/shell or hollow micro and nanofibers of a broad variety of materials, a process termed co-electrospinning. However, we shall restrict ourselves in the foregoing to applications in which particles are sought.

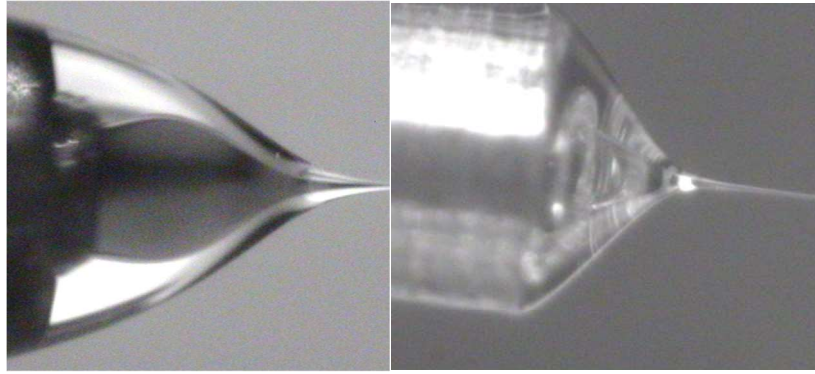


Fig. 15. Pictures of a compound Taylor cone and the core-shell jet issued from its tip. Courtesy of I.G. Loscertales. Left: Somos® outside and ethylene glycol (stained) inside. Right: olive oil outside and water (inside).

The dynamics of compound steady cone-jet electrospays has been studied experimentally and theoretically. To form the compound Taylor cone at least one of the liquids must have certain electrical conductivity. If the outer liquid is a dielectric, then the electric field penetrates through it and the induced charges lay on the inner liquid-liquid interface, where the electric stresses act. In this case, the core liquid is called the *driving liquid*. On the other hand, if the sheath liquid has some electric conductivity the electric stresses would only act on its outermost surface, and it would be the driving liquid. In either case, there exists an interface which is set into motion by the electric stresses. This motion must be propagated into both fluids, such that both develop a main velocity towards the apex of the compound Taylor cone. Viscosity becomes essential in setting up these velocities, especially when the driving liquid is the shell fluid. In this case, since the electric stresses do not penetrate down to the core liquid, it is the motion of the shell liquid towards the apex who must exert mechanical (i.e. viscous) stresses on the liquid-liquid interface to overcome the interfacial tension that resists the elongation of the core liquid meniscus towards the apex. López-Herrera et al. (2003) reported the scaling laws for the emitted current and droplet size of coaxial electrospays. Similarly to regular electrospays, the properties of the driving fluid must be the ones used to evaluate the proposed scaling for the current, and both flow rates (core and shell liquids) must be taken into account to predict the droplet diameter, as well as the sum of the surface tension of both inner and outer interfaces. Chen et al. (2005) experimentally studied the different EHD modes in the coaxial configuration, and found similar modes as those for single liquid EHD spraying, namely, as the applied voltage is increased: dripping, intermittent

cone-jet, steady cone-jet and multi jet. They also noticed that the properties of the shell liquid (the driving liquid in their case), rather than the core liquid, determined the outcome. Li et al. (2006a, 2006b) were the first to theoretically analyze the linear stability of a coaxial jet under axial and radial electric fields. In brief, these authors analyze three axisymmetric modes, the paravaricose (out of phase), the parasinuous (in phase) and the transitional mode (changing continuously from in phase to out of phase) for the case of inviscid liquids, and four different combinations of electric properties of the liquids: dielectric-conductor, conductor-dielectric, conductor-conductor and dielectric-dielectric. They find that the strength of the axial electric field, E , and the jet Weber number, We , have a very strong effect on the stability of the compound jet. In their We - E instability map, most of it is of the parasinuous mode, which is the most frequently observed experimentally. Higuera (2007) studied the stationary flow of an electrified coaxial jet of viscous fluids with the driving fluid outside, including the leaky dielectric model for charge transport within (Saville, 1997), and the quasi-unidirectional approximation. He analyzed the current transfer region, where it shifts from conduction to convection current, and also studied the effect of some parameters, such as the viscosity ratio, on the ranges of operation where steady coaxial jets are possible. Further insights on the EHD are considered in Higuera (2018). Mei & Chen (2007) experimentally studied the effect of surface tension on the encapsulation efficiency of the coaxial electrospray process. Li et al. (2008) also included a finite conductivity in their stability analysis of electrified coaxial jets. Marín et al. (2008) analyzed the formation of steady conical tips of dielectric fluids inside Taylor cones of conducting liquids, proposing a simplified model to explain their observations. Si et al. (2012) and Si et al. (2013) studied experimentally and theoretically the stability of electrified coaxial jets, aiming at synthesizing microparticles encapsulating imaging and therapeutic agents. Zhang et al. (2012a) reviewed advances towards controlling the coaxial electrospray process as a tool for synthesizing microparticles for medical applications. Luo & Edirisinghe (2014) used a liquid core in coaxial electrospray to control the transition from electrospraying to electrospinning. More recently, Sofokleous et al. (2016) looked at the effect of the axial location of the inner needle in the coaxial nozzle upon the robustness of the coaxial electrospray process. Li et al. (2016) analyzed the absolute and convective instability of coaxial viscous jets under axial and radial electric fields, with the aim of predicting parametrical regions where the non-axisymmetric (whipping) instability may be suppressed in favor of the parasinuous mode. Yan et al. (2016) attempted direct numerical simulation (CFD) of the

cone-jet in coaxial electro-hydrodynamic atomization (CEHD). Their results agreed with experimental data. They realized that the use of almost miscible liquids, that is, reducing the liquid-liquid interfacial tension, eases the operation of CEHD. These authors also suggest that the use of conically shaped nozzles allow increasing the total liquid flow rate and so the throughput. The same authors also analyze the problem of upscaling CEHD (Yan et al., 2017). They propose a multi-scale model to interpret their experimental results with an injector consisting of two nozzles. Other attempts to upscale CEHD have been reported by Srivastava et al. (2007) and by Olvera-Trejo & Velásquez-García (2016). The former designed and built a microfluidic manifold with four coaxial micro nozzles capable that was tested to synthesize hollow fibers of certain polymers. The later used 3D printing to build a miniaturized chip with 25 coaxial nozzles with a density of 25 nozzles per squared cm. He et al. (2005) reviewed potential industrial applications of the core-shell structures created by CE. Marín et al. (2007) proved that CE could be set inside dielectric liquid baths instead of air.

The coaxial electrospray (CE) has been applied to the synthesis of particles for applications in many technological fields. Among those, one may point out Food Technology (Bocanegra et al. (2005), Koo (2014), Bakry et al. (2016), etc.) or Drug delivery (Yoo et al. (2007), Yoon et al. (2008), Xu & Hanna (2008), Chakraborty et al. (2009), Wu et al. (2009), (Wu et al., 2010), Wu et al. (2010b), Zamani et al. (2013), Zamani et al. (2014), Zamani et al. (2015), among others) among many others. Enayati et al. (2011) published a review on the biomedical applications of CE encapsulation, highlighting its benefits for encapsulation of active, delicate substances like drugs, enzymes, proteins, antibiotics or DNA fragments, among others. Many groups have confirmed the benefits of the core-shell capsules formed by CE to control the release profile of such capsules (Xu et al. (2013), Lee et al. (2010), Wang et al. (2013), Cui et al. (2014), Chen et al. (2018), Cao et al. (2017), and Li et al. (2017), among others.), noticing also the benefits of such capsules to improve the uptake and effectiveness of poorly soluble drugs (Zhang et al. (2011), Kawakami (2013), Hao et al. (2014), Liu et al. (2014, among others). The CE technology has been also used to synthesize active or smart particles (Jing et al. (2011), Park et al. (2011), Park et al. (2011b), Yang et al. (2013), among others), highly efficient dye-sensitized solar cells for energy harvesting (Xi et al. (2012) and Anjusree et al. (2005), among others) or even nanocrystals of rare earths, De

Cárcer et al. (2005). Biotechnology, cell encapsulation and cell harvesting has been other area in which CE has shown a great potential (Laelorspoen et al. (2014), Cao et al. (2014a and 2014b), Zhao et al. (2014), Castro et al. (2014), Bae & Lee (2014) among others). Anti-cancer and other therapies had been successfully performed with capsules formed by CE (Kim et al. (2015), Zhu et al. (2016), Kim et al. (2013), Cao et al. (2014c), Cao et al. (2014d), Zhu et al. (2016), Guan et al. (2016), Ho et al. (2017) and Li et al. (2017), Zhang et al. (2012 b), among others). These accomplishments are broadened by the development of novel collection strategies of the liquid core-shell capsules, which allows more degree of freedom and control of the final product (Kim & Lee (2011), Zhang et al. (2012c), Gao (2015), among others).

Nevertheless, despite of the potential of the coaxial electrospray for micro and nanoencapsulation of labile substances, it still remains a relatively unexplored tool, susceptible of much improvement. Little efforts have been directed, for example, towards the upscaling of CE in order to make this tool attractive to industry. Further understanding of this complex electro-hydrodynamic process is still needed, process that becomes even more involved when the interaction of the different chemical components affects the fluid-fluid properties. Therefore, it becomes a truly interdisciplinary problem that, perhaps, may be intriguing enough to attract the interest of researches from many different areas.

5. Conclusions

We have presented a review focused on the fundamentals of electrospraying, also known as electrohydrodynamic atomization and electrohydrodynamic spraying. We have described the different fluid dynamic modes and regimes developing in liquid menisci to which an electrical potential is applied. We have provided objective criteria to differentiate the different modes, and have described parametric operation windows by reference to dimensionless numbers. Such objective criteria should be helpful for identifying modes in future electrospray literature. The recent affordability of high speed video has stimulated its use for carrying out detailed characterizations of unsteady modes, and it is a promising methodology for future research in this area, especially when combined with other techniques (e.g. fast electrical current measurement). From the point of view of applications, the mode of greatest interest thus far has been the cone-jet mode

in which the electrified meniscus adopts a conical shape, emitting a steady microscopic jet which leads to uniformly sized droplets. We have described the physics of this mode in detail, first by reviewing the remarkable effort in the field to identify so-called scaling laws. These are simple scaling relationships connecting the variables of the problem, which can be applicable to many operating conditions. We have then described the dynamics of generation of the jet which emerges from the electrified conical meniscus, as well as the physics associated with the spray structure development. Finally, we have presented an extension of these concepts for multi-fluid configurations, such as coaxial and parallel flows. The coaxial electrospray methodology still remains relatively unexplored as a tool for encapsulation of labile substances, where much future improvement and further research on the underlying physical phenomena are expected. As applications of electrospray continue to develop, research on the underlying mechanisms will likely provide helpful insights for making this complex system reliable and robust in practical production settings.

Acknowledgements

This work has been supported by the Spanish MINECO under grants DPI2017-86547-C2-1-P, DPI2015-68969-P, and DPI2015-71901-REDT, by the Catalan government under grant 2017SGR1516, and by Universitat Rovira i Virgili through grant 2015PFR-URV-B2-57.

References

- Abramzon, B. and Sirignano, W. A. (1989). Droplet Vaporization Model for Spray Combustion Calculations. *Int. J. Heat Mass Transf.*, 32(9):1605–1618.
- Achtzehn, T., Müller, R., Duft, D., & Leisner, T. (2005). The Coulomb instability of charged microdroplets: dynamics and scaling. *European Physical Journal D*, 34(1), 311–313. <http://doi.org/10.1140/epjd/e2005-00102-1>
- Agostinho, L. L. F., Tamminga, G., Yurteri, C. U., Brouwer, S. P., Fuchs, E. C., & Marijnissen, J. C. M. (2012a). Morphology of water electrosprays in the simple-jet mode. *Phys. Rev. E*, 86(6), 066317 (9pp). <https://doi.org/10.1103/PhysRevE.86.066317>
- Agostinho, L. L. F., Yurteri, C. U., Fuchs, E. C., & Marijnissen, J. C. M. (2012b). Monodisperse water microdroplets generated by electrohydrodynamic atomization in the simple-jet mode. *Applied Physics Letters*, 100(24), 7–11. <http://doi.org/10.1063/1.4729021>
- Aguirre-de-Carcer, I., & Fernández de la Mora, J. (1995). Effect of background gas on the current emitted from Taylor cones. *Journal of Colloid and Interface Science*. <https://doi.org/10.1006/jcis.1995.1210>

- Anjusree, G.S., Deepak, T.G., Nair, S.V., Nair, A.S. Facile fabrication of TiO₂ nanoparticle-TiO₂ nanofiber composites by co-electrospinning-electrospraying for dye-sensitized solar cells (2015) *Journal of Energy Chemistry*, 24 (6), pp. 762-769.
- Arumugham-Achari, A. K., Grifoll, J., & Rosell-Llompart, J. (2013). Two-way coupled numerical simulation of electrospray with induced gas flow. *Journal of Aerosol Science*, 65, 121–133. <https://doi.org/10.1016/j.jaerosci.2013.07.005>
- Arumugham-Achari, A. K., Grifoll, J., & Rosell-Llompart, J. (2015). A comprehensive framework for the numerical simulation of evaporating electrosprays. *Aerosol Science and Technology*, 49(6), 436–448. <https://doi.org/10.1080/02786826.2015.1039639>
- Asano, K., & Yatsuzuka, K. (1999). Rotational motion of water ligament drawn by electrostatic force. *Journal of Electrostatics*, 46(2), 69–77. [https://doi.org/https://doi.org/10.1016/S0304-3886\(99\)00017-0](https://doi.org/https://doi.org/10.1016/S0304-3886(99)00017-0)
- Bae, H., Lee, J. Encapsulated particles attached on electrospun fibers by in situ combination of electrospinning and coaxial electrospraying (2014) *Journal of Nanoscience and Nanotechnology*, 14 (10), pp. 7574-7580
- Bakry, A.M., Abbas, S., Ali, B., Majeed, H., Abouelwafa, M.Y., Mousa, A., Liang, L. Microencapsulation of Oils: A Comprehensive Review of Benefits, Techniques, and Applications (2016) *Comprehensive Reviews in Food Science and Food Safety*, 15 (1), pp. 143-182.
- Barrero, A., Gañán-Calvo, A. M., Dávila, J., Palacio, A., & Gómez-González, E. (1998). Low and high Reynolds number flows inside Taylor cones. *Phys. Rev. E*, 58(6), 7309–7314. <https://doi.org/10.1103/PhysRevE.58.7309>
- Barrero, A., Gañán-Calvo, A. M., Dávila, J., Palacios, A., & Gómez-González, E. (1999). The role of the electrical conductivity and viscosity on the motions inside Taylor cones. *Journal of Electrostatics*, 47(1), 13–26. [https://doi.org/https://doi.org/10.1016/S0304-3886\(99\)00021-2](https://doi.org/https://doi.org/10.1016/S0304-3886(99)00021-2)
- Barrero, A., & Loscertales, I. G. (2007). Micro- and Nanoparticles via Capillary Flows. *Annual Review of Fluid Mechanics*, 39(1), 89–106. <https://doi.org/10.1146/annurev.fluid.39.050905.110245>
- Barrios-Collado, C., Vidal-De-Miguel, G., & Martínez-Lozano Sinues, P. (2016). Numerical modeling and experimental validation of a universal secondary electrospray ionization source for mass spectrometric gas analysis in real-time. *Sensors and Actuators, B: Chemical*, 223, 217–225. <https://doi.org/10.1016/j.snb.2015.09.073>
- Basak, S., Chen, D. R. and Biswas, P. (2007). Electrospray of ionic precursor solutions to synthesize iron oxide nanoparticles: Modified scaling law. *Chem. Eng. Sci.*, 62(4), 1263–1268. <http://doi.org/10.1016/j.ces.2006.11.029>
- Bober, D. B., & Chen, C.-H. (2011). Pulsating electrohydrodynamic cone-jets: from choked jet to oscillating cone. *Journal of Fluid Mechanics*, 689, 552–563. <http://doi.org/10.1017/jfm.2011.453>
- Bocanegra, R., Gaonkar, A.G., Barrero, A., Loscertales, I.G., Pechack, D., Marquez, M. Production of cocoa butter microcapsules using an electrospray process (2005) *Journal of Food Science*, 70 (8), pp. E492-E497.
- Bock, N., Dargaville, T. R., & Woodruff, M. A. (2012). Electrospraying of polymers with therapeutic molecules: State of the art. *Progress in Polymer Science*, 37(11), 1510–1551. <http://doi.org/10.1016/j.progpolymsci.2012.03.002>
- Bodnár, E., & Rosell-Llompart, J. (2013). Growth dynamics of granular films produced by electrospray. *Journal of Colloid and Interface Science*, 407, 536–545. <https://doi.org/10.1016/j.jcis.2013.06.013>
- Borra, J. P., Ehouarn, P., & Boulaud, D. (2004). Electrohydrodynamic atomisation of water stabilised by glow discharge - Operating range and droplet properties. *Journal of Aerosol Science*, 35(11), 1313–1332. <http://doi.org/10.1016/j.jaerosci.2004.05.011>
- Borra, J. P., Tombette, Y., & Ehouarn, P. (1999). Influence of electric field profile and polarity on the mode of EHDA related to electric discharge regimes. *Journal of Aerosol Science*, 30(7), 913–925. [https://doi.org/10.1016/S0021-8502\(98\)00779-4](https://doi.org/10.1016/S0021-8502(98)00779-4)

- Cao, L., Luo, J., Tu, K., Wang, L.-Q., Jiang, H. Generation of nano-sized core-shell particles using a coaxial tri-capillary electrospray-template removal method (2014a) *Colloids and Surfaces B: Biointerfaces*, 115, pp. 212-218.
- Cao, L.-H., Wang, H.-J., Tu, K.-H., Jiang, H.-L., Wang, L.-Q. Core-shell nanoparticles fabricated by tri-capillary coaxial electrospray and template removal method for protein delivery (2014b) *Acta Polymerica Sinica*, (9), pp. 1238-1243.
- Cao, Y., Liu, F., Chen, Y., Yu, T., Lou, D., Guo, Y., Li, P., Wang, Z., Ran, H. Drug release from core-shell PVA/silk fibroin nanoparticles fabricated by one-step electrospraying (2017) *Scientific Reports*, 7 (1), art. no. 11913
- Cao, Y., Wang, B., Wang, Y., Lou, D. Dual drug release from core-shell nanoparticles with distinct release profiles (2014c) *Journal of Pharmaceutical Sciences*, 103 (10), pp. 3205-3216
- Cao, Y., Wang, B., Wang, Y., Lou, D. Polymer-controlled core-shell nanoparticles: A novel strategy for sequential drug release (2014d) *RSC Advances*, 4 (57), pp. 30430-30439
- Carretero, J., & Martínez-Sánchez, M. (2004). Numerical simulation of a colloidal thruster in the droplet regime. *Computer Physics Communications*, 164(1–3), 202–208. <https://doi.org/10.1016/j.cpc.2004.06.074>
- Castellanos, A. *Electrohydrodynamics*. Springer. 1998.
- Castro, N.J., O'Brien, C.M., Zhang, L.G. Biomimetic biphasic 3-D nanocomposite scaffold for osteochondral regeneration (2014) *AIChE Journal*, 60 (2), pp. 432-442.
- Chakraborty, S., Liao, I.-C., Adler, A., Leong, K.W. Electrohydrodynamics: A facile technique to fabricate drug delivery systems (2009) *Advanced Drug Delivery Reviews*, 61 (12), pp. 1043-1054
- Chen, D.-R., Wendt, H., Pui, D.Y.H. (2000). A novel approach for introducing Bio-materials into cells. *Journal of Nanoparticle Research*, 2 (2), 133-139.
- Chen, D. R., Pui, D. Y. H., & Kaufman, S. L. (1995). Electro spraying of conducting liquids for monodisperse aerosol generation in the 4 nm to 1.8 μ m diameter range. *Journal of Aerosol Science*, 26(6), 963–977. [https://doi.org/10.1016/0021-8502\(95\)00027-A](https://doi.org/10.1016/0021-8502(95)00027-A)
- Chen, D.-R. and Pui, D. Y. H. (1997) Experimental investigation of scaling laws for electro spraying: dielectric constant effect. *Aerosol Sci. and Technol.*, 27, 367-380.
- Chen, J., Cao, L., Cui, Y., Tu, K., Wang, H., Wang, L.-Q. The exploration of endocytic mechanisms of PLA-PEG nanoparticles prepared by coaxial tri-capillary electrospray-template removal method (2018) *Colloids and Surfaces B: Biointerfaces*, 161, pp. 10-17.
- Chen, X., Jia, L., Yin, X., Cheng, J., Lu, J. Spraying modes in coaxial jet electrospray with outer driving liquid (2005) *Physics of Fluids*, 17 (3), pp. 032101-1-032101-7.
- Cherney, L. T. (1999a). Structure of Taylor cone-jets: limit of low flow rates. *Journal of Fluid Mechanics*, 378, 167–196.
- Cherney, L. T. (1999b). Electrohydrodynamics of electrified liquid menisci and emitted jets. *Journal of Aerosol Science*, 30(7), 851–862. [https://doi.org/10.1016/S0021-8502\(98\)00756-3](https://doi.org/10.1016/S0021-8502(98)00756-3)
- Clanet, C., & Lasheras, J. C. (1999). Transition from dripping to jetting. *Journal of Fluid Mechanics*, 383, 307–326. <https://doi.org/10.1017/S0022112098004066>
- Clift, R., Grace, J.R. & Weber, M.E. (1978). *Bubbles, drops, and particles*. Academic Press: New York.
- Cloupeau, M., & Prunet-Foch, B. (1989). Electrostatic spraying of liquids in cone-jet mode. *Journal of Electrostatics*, 22(2), 135–159. [http://doi.org/10.1016/0304-3886\(89\)90081-8](http://doi.org/10.1016/0304-3886(89)90081-8)
- Cloupeau, M., & Prunet-Foch, B. (1990). Electrostatic spraying of liquids: Main functioning modes. *Journal of Electrostatics*, 25(2), 165–184. [http://doi.org/http://dx.doi.org/10.1016/0304-3886\(90\)90025-Q](http://doi.org/http://dx.doi.org/10.1016/0304-3886(90)90025-Q)
- Crowe, C., Sommerfeld, M. and Tsuji, Y. (1998) *Multiphase flows with droplets and particles*, CRC Press, Boca Raton.
- Cui, L., Liu, Z.-P., Yu, D.-G., Zhang, S.-P., Bligh, S.W.A., Zhao, N. Electro sprayed core-shell nanoparticles of PVP and shellac for furnishing biphasic controlled release of ferulic acid (2014) *Colloid and Polymer Science*, 292 (9), pp. 2089-2096.

- Dastourani, H., Jahannama, M. R., & Eslami-Majd, A. (2018). A physical insight into electro-spray process in cone-jet mode: Role of operating parameters. *International Journal of Heat and Fluid Flow*, 70, 315–335.
<https://doi.org/10.1016/j.ijheatfluidflow.2018.02.012>
- De Cárcer, I.A., Herrero, P., Landa-Cánovas, A.R., Sobolev, B. Nanocrystals of cerium and europium trifluorides generated by coaxial Taylor cone electro-spray of aqueous solutions at room temperature (2005) *Applied Physics Letters*, 87 (5), art. no. 053105,
- de Juan, L., & Fernández de la Mora, J. (1997). Charge and size distributions of electro-spray drops. *Journal of Colloid and Interface Science*, 186, 280–293.
<https://doi.org/10.1006/jcis.1996.4654>
- Deng, W., & Gomez, A. (2007). Influence of space charge on the scale-up of multiplexed electro-sprays. *Journal of Aerosol Science*, 38(10), 1062–1078.
<https://doi.org/10.1016/j.jaerosci.2007.08.005>
- Dunn, P. F., & Snarski, S. R. (1992). Droplet diameter, flux, and total current measurements in an electrohydrodynamic spray. *Journal of Applied Physics*, 71(1), 80–84.
<https://doi.org/10.1063/1.350651>
- Dunn, P. F., Grace, J. M., & Snarski, S. R. (1994). The mixing of electrically-charged droplets between and within electrohydrodynamic fine sprays. *Journal of Aerosol Science*, 25(6), 1213–1227. [https://doi.org/http://dx.doi.org/10.1016/0021-8502\(94\)90210-0](https://doi.org/http://dx.doi.org/10.1016/0021-8502(94)90210-0)
- Eggers, J. (1997). Nonlinear dynamics and breakup of free-surface flows. *Reviews of Modern Physics*, 69(3), 865–930. <https://doi.org/10.1103/RevModPhys.69.865>
- Eggers, J., & Villermaux, E. (2008). Physics of liquid jets. *Reports on Progress in Physics*, 71(3), 036601 (79pp). <https://doi.org/10.1088/0034-4885/71/3/036601>
- Enayati, M., Chang, M.-W., Bragman, F., Edirisinghe, M., Stride, E. Electrohydrodynamic preparation of particles, capsules and bubbles for biomedical engineering applications (2011) *Colloids and Surfaces A: Physicochemical and Engineering Aspects*, 382 (1-3), pp. 154-164
- Fenn, J. B. (2003). Electro-spray wings for molecular elephants (Nobel lecture). *Angewandte Chemie International Edition*, 42, 3871–3894. <http://doi.org/10.1002/anie.200300605>
- Fenn, J. B., Mann, M., Meng, C. K., Wong, S. F., & Whitehouse, C. M. (1989). Electro-spray ionization for mass spectrometry of large biomolecules. *Science*, 246(4926), 64–71.
<http://science.sciencemag.org/content/246/4926/64.abstract>
- Fernandez de la Mora, J., Navascues, J., Fernandez, F., & Rosell-Llompart, J. (1990). Generation of submicron monodisperse aerosols in electro-sprays. *Journal of Aerosol Science*, 21(SUPPL. 1), S673–S676. [https://doi.org/10.1016/0021-8502\(90\)90332-R](https://doi.org/10.1016/0021-8502(90)90332-R)
- Fernández de la Mora, J. (1992). The effect of charge emission from electrified liquid cones. *Journal of Fluid Mechanics*, 243, 561–574. <https://doi.org/DOI:10.1017/S0022112092002829>
- Fernández de la Mora, J. (2007). The fluid dynamics of Taylor cones. *Annual Review of Fluid Mechanics*, 39(1), 217–243. <https://doi.org/10.1146/annurev.fluid.39.050905.110159>
- Fernández de la Mora, J., & Loscertales, I. G. (1994). The current emitted by highly conducting Taylor cones. *Journal of Fluid Mechanics*, 260, 155–184. <https://doi.org/DOI:10.1017/S0022112094003472>
- Forbes, T. P., Degertekin, F. L., & Fedorov, A. G. (2010). Electrohydrodynamics of charge separation in droplet-based ion sources with time-varying electrical and mechanical actuation. *Journal of the American Society for Mass Spectrometry*, 21(4), 501–510.
<http://doi.org/10.1016/j.jasms.2009.12.022>
- Gamero-Castaño, M. (2008). The structure of electro-spray beams in vacuum. *Journal of Fluid Mechanics*, 604, 339–368. <https://doi.org/10.1017/S0022112008001316>
- Gamero-Castaño, M. and Hruby, V. (2002). Electric measurements of charged sprays emitted by cone-jets. *J. Fluid Mech.*, 459, 245–276. <http://doi.org/10.1017/S002211200200798X>
- Gañán-Calvo, A. (1997). Cone-jet analytical extension of Taylor’s electrostatic solution and the asymptotic universal scaling laws in electro-spraying. *Physical Review Letters*, 79(2), 217–220. <https://doi.org/10.1103/PhysRevLett.79.217>

- Gañán-Calvo, A. (1999) The surface charge in electrospraying: its nature and its universal scaling laws. *J. Aerosol Sci.*, 30(7) 863-872.
- Gañán-Calvo, A. M. (2004). On the general scaling theory for electrospraying. *J. Fluid Mech.*, 507, 203–212a. <http://doi.org/10.1017/S0022112004008870>.
- Gañán-Calvo, A. M., & Montanero, J. M. (2009). Revision of capillary cone-jet physics: Electrospray and flow focusing. *Physical Review E - Statistical, Nonlinear, and Soft Matter Physics*, 79(6), 1–18. <https://doi.org/10.1103/PhysRevE.79.066305>
- Gañán-Calvo, A. M., Lasheras, J. C., Dávila, J., & Barrero, A. (1994). The electrostatic spray emitted from an electrified conical meniscus. *Journal of Aerosol Science*, 25(6), 1121–1142. [https://doi.org/10.1016/0021-8502\(94\)90205-4](https://doi.org/10.1016/0021-8502(94)90205-4)
- Gañán-Calvo, A. M., Rebollo-Muñoz, N., & Montanero, J. M. (2013). The minimum or natural rate of flow and droplet size ejected by Taylor cone-jets: Physical symmetries and scaling laws. *New J. Phys.*, 15. <http://doi.org/10.1088/1367-2630/15/3/033035>
- Gañán-Calvo, Dávila, J. and Barrero, A. (1997) Current and droplet size in the electrospraying of liquids scaling laws. *J. Aerosol Sci.*, 28(2), 249-275.
- Gao, Y., Zhao, D., Chang, M.-W., Ahmad, Z., Li, X., Suo, H., Li, J.-S. Morphology control of electrosprayed core-shell particles via collection media variation (2015) *Materials Letters*, 146, pp. 59-64.
- Garton, C. G., & Krasucki, Z. (1964). Bubbles in insulating liquids: stability in an electric field. *Proceedings of the Royal Society of London A: Mathematical, Physical and Engineering Sciences*, 280(1381), 211–226. <https://doi.org/10.1098/rspa.1964.0141>
- Gomez, A., & Tang, K. (1991). Characterization of a high charge density electrospray of methanol. In *Fifth International Conference on Liquid Atomization and Spray Systems, ICLASS-91*. Gaithersburg MD.
- Gomez, A., & Tang, K. (1994). Charge and fission of droplets in electrostatic sprays. *Physics of Fluids*, 6(1), 404–414. <https://doi.org/10.1063/1.868037>
- Grace, J. M., & Dunn, P. F. (1996). Droplet motion in an electrohydrodynamic fine spray. *Experiments in Fluids*, 20(3), 153–164. <https://doi.org/10.1007/BF00190271>
- Grace, J. M., & Marijnissen, J. C. M. (1994). A review of liquid atomization by electrical means. *Journal of Aerosol Science*, 25(6), 1005–1019. [http://doi.org/10.1016/0021-8502\(94\)90198-8](http://doi.org/10.1016/0021-8502(94)90198-8)
- Grifoll, J., & Rosell-Llompart, J. (2012). Efficient Lagrangian simulation of electrospray droplets dynamics. *Journal of Aerosol Science*, 47, 78–93.
- Grifoll, J., & Rosell-Llompart, J. (2014). Continuous droplets' charge method for the Lagrangian simulation of electrostatic sprays. *Journal of Electrostatics*, 72(5), 357–364.
- Guan, Y., Zhou, Y., Sheng, J., Ying Jiang, Z., Jumahan, H., Hu, Y. Preparation of ALA-loaded PLGA nanoparticles and its application in PDT treatment (2016) *Journal of Chemical Technology and Biotechnology*, 91 (4), pp. 1128-1135
- Hao, S., Wang, B., Wang, Y., Xu, Y. Enteric-coated sustained-release nanoparticles by coaxial electrospray: Preparation, characterization, and in vitro evaluation (2014) *Journal of Nanoparticle Research*, 16 (2), art. no. 2204
- Hartman, R. P. A., Borra, J. P., Brunner, D. J., Marijnissen, J. C. M., & Scarlett, B. (1999b). The evolution of electrohydrodynamic sprays produced in the cone-jet mode, a physical model. *Journal of Electrostatics*, 47(3), 143–170. [https://doi.org/10.1016/S0304-3886\(99\)00034-0](https://doi.org/10.1016/S0304-3886(99)00034-0)
- Hartman, R. P. A., Brunner, D. J., Camelot, D. M. A., Marijnissen, J. C. M., & Scarlett, B. (1999a). Electrohydrodynamic atomization in the cone-jet mode physical modeling of the liquid cone and jet. *Journal of Aerosol Science*, 30(7), 823–849. [https://doi.org/10.1016/S0021-8502\(99\)00033-6](https://doi.org/10.1016/S0021-8502(99)00033-6)
- Hartman, R. P. A., Brunner, D. J., Camelot, D. M. A., Marijnissen, J. C. M., & Scarlett, B. (2000). Jet break-up in electrohydrodynamic atomization in the cone-jet mode. *Journal of Aerosol Science*, 31(1), 65–95. [https://doi.org/10.1016/S0021-8502\(99\)00034-8](https://doi.org/10.1016/S0021-8502(99)00034-8)
- Hayati, I., Bailey, A., & Tadros, Th. F. (1987). Investigations into the mechanism of electrohydrodynamic spraying of liquids: II. Mechanism of stable jet formation and

- electrical forces acting on a liquid cone. *Journal of Colloid and Interface Science*, 117(1), 222–230. [http://doi.org/https://doi.org/10.1016/0021-9797\(87\)90186-X](http://doi.org/https://doi.org/10.1016/0021-9797(87)90186-X)
- He, C., Huang, Z., Han, X., Liu, L., Hu, Y., Zhang, Y. Recent development of the nanocomposites prepared by coaxial jet technology (2005) *Fuhe Cailiao Xuebao/Acta Materiae Compositae Sinica*, 22 (6), pp. 1-8.
- Higuera, F. J. (2003). Flow rate and electric current emitted by a Taylor cone. *Journal of Fluid Mechanics*, 484, 303–327. <https://doi.org/10.1017/S0022112003004385>
- Higuera, F. J. (2004). Current/flow-rate characteristic of an electrospray with a small meniscus. *Journal of Fluid Mechanics*, 513, 239–246. <https://doi.org/10.1017/S0022112004000308>
- Higuera, F. J. (2012). Eulerian model of a dilute spray of charged droplets. *Journal of Aerosol Science*, 48, 34–45. <https://doi.org/10.1016/j.jaerosci.2012.01.008>
- Higuera, F. J. (2013). Multifluid Eulerian model of an electrospray in a host gas. *Journal of Fluid Mechanics*, 734, 363–386. <https://doi.org/10.1017/jfm.2013.450>
- Higuera, F. J. (2016a). Dispersion and vaporization of a dilute spray of electrified droplets injected in a coflowing hot gas - Application to the vaporization chamber of a minicombustor. *Journal of Aerosol Science*, 91, 78–93. <https://doi.org/10.1016/j.jaerosci.2015.09.009>
- Higuera, F. J. (2016b). Neutralization of a spray of electrically charged droplets by a corona discharge. *Journal of Fluid Mechanics*, 801, 130–149. <https://doi.org/10.1017/jfm.2016.449>
- Higuera, F. J. (2017). Qualitative analysis of the minimum flow rate of a cone-jet of a very polar liquid. *Journal of Fluid Mechanics*, 816, 428–441. <https://doi.org/10.1017/jfm.2017.111>
- Higuera, F. J. and Barrero, A. (2005). Electrosprays of very polar liquids at low flow rates. *Phys. Fluids*, 17(1). <https://doi.org/10.1063/1.1824491>
- Higuera, F. J., & Tejera, J. M. (2017). Vaporization and gas-phase combustion of electrosprayed heptane in a small chamber. *Combustion and Flame*, 177, 144–154. <https://doi.org/10.1016/j.combustflame.2016.12.015>
- Higuera, F.J. Electric field effects (2018) *Fluids, Colloids and Soft Materials: An Introduction to Soft Matter Physics*, pp. 19-28.
- Higuera, F.J. Stationary coaxial electrified jet of a dielectric liquid surrounded by a conductive liquid (2007) *Physics of Fluids*, 19 (1), art. no. 012102,
- Higuera, J. F. (2009). Charge separation in the conical meniscus of an electrospray of a very polar liquid: Its effect on the minimum flow rate. *Physics of Fluids*, 21(3), 032104 (11pp). <https://doi.org/10.1063/1.3088491>
- Hijano, A. J., Loscertales, I. G., Ibáñez, S. E., & Higuera, F. J. (2015). Periodic emission of droplets from an oscillating electrified meniscus of a low-viscosity, highly conductive liquid. *Physical Review E - Statistical, Nonlinear, and Soft Matter Physics*, 91(1), 013011 (12pp). <http://doi.org/10.1103/PhysRevE.91.013011>
- Hinds, W. C. (1999) *Aerosol Technology, Properties, Behavior, and Measurement of Airborne Particles*, 2nd ed.; John Wiley & Sons: New York.
- Ho, H.N., Laidmäe, I., Kogermann, K., Lust, A., Meos, A., Nguyen, C.N., Heinämäki, J. Development of electrosprayed artesunate-loaded core-shell nanoparticles (2017) *Drug Development and Industrial Pharmacy*, 43 (7), pp. 1134-1142
- Hogan, C. J., & Biswas, P. (2008). Porous film deposition by electrohydrodynamic atomization of nanoparticle sols. *Aerosol Science and Technology*, 42(1), 75–85. <https://doi.org/10.1080/02786820701787951>
- Huebner, A. L., & Chu, H. N. (1971). Instability and breakup of charged liquid jets. *Journal of Fluid Mechanics*, 49(2), 361–372. <https://doi.org/10.1017/S002211207100212X>
- Jaworek, A. (2007a). Micro- and nanoparticle production by electrospraying. *Powder Technology*, 176(1), 18–35. <http://doi.org/10.1016/j.powtec.2007.01.035>
- Jaworek, A. (2007b). Electrospray droplet sources for thin film deposition. *Journal of Materials Science*, 42(1), 266–297. <https://doi.org/10.1007/s10853-006-0842-9>
- Jaworek, A., & Krupa, A. (1996). Generation and characteristics of the precession mode of EHD spraying. *Journal of Aerosol Science*, 27(1), 75–82. [http://doi.org/10.1016/0021-8502\(95\)00528-5](http://doi.org/10.1016/0021-8502(95)00528-5)

- Jaworek, A., & Krupa, A. (1997). Studies of the corona discharge in ehd spraying. *Journal of Electrostatics*, 40–41, 173–178. [http://doi.org/10.1016/S0304-3886\(97\)00033-8](http://doi.org/10.1016/S0304-3886(97)00033-8)
- Jaworek, A., & Krupa, A. (1999). Classification of the modes of EHD spraying. *Journal of Aerosol Science*, 30(7), 873–893. [http://doi.org/10.1016/S0021-8502\(98\)00787-3](http://doi.org/10.1016/S0021-8502(98)00787-3)
- Jaworek, A., & Sobczyk, A. T. (2008). Electro spraying route to nanotechnology: An overview. *Journal of Electrostatics*, 66(3–4), 197–219. <http://doi.org/10.1016/j.elstat.2007.10.001>
- Jaworek, A., Sobczyk, A., Czech, T., & Krupa, A. (2014). Corona discharge in electro spraying. *Journal of Electrostatics*, 72(2), 166–178. <http://doi.org/10.1016/j.elstat.2014.01.004>
- Jing, Y., Zhu, Y., Yang, X., Shen, J., Li, C. Ultrasound-triggered smart drug release from multifunctional core-shell capsules one-step fabricated by coaxial electro spray method (2011) *Langmuir*, 27 (3), pp. 1175-1180.
- Jung, J. H., Oh, H., & Kim, S. S. (2010). Numerical simulation of the deposition pattern in multiple electrohydrodynamic spraying. *Powder Technology*, 198(3), 439–444. <https://doi.org/10.1016/j.powtec.2009.12.006>
- Juraschek, R., & Röllgen, F. W. (1998). Pulsation phenomena during electro spray ionization. *International Journal of Mass Spectrometry*, 177(1), 1–15. [http://doi.org/10.1016/s1387-3806\(98\)14025-3](http://doi.org/10.1016/s1387-3806(98)14025-3)
- Kaiser, S., Kyritsis, D. C., Dobrowolski, P., Long, M. B., & Gomez, A. (2003). The electro spray and combustion at the mesoscale. *Journal of the Mass Spectrometry Society of Japan*, 51(1), 42–49. <https://doi.org/10.5702/massspec.51.42>
- Kawakami, K., Zhang, S., Chauhan, R.S., Ishizuka, N., Yamamoto, M., Masaoka, Y., Kataoka, M., Yamashita, S., Sakuma, S. Preparation of fenofibrate solid dispersion using electro spray deposition and improvement in oral absorption by instantaneous post-heating of the formulation (2013) *International Journal of Pharmaceutics*, 450 (1-2), pp. 123-128.
- Kim, H., Kim, J., Yang, H., Suh, J., Kim, T., Han, B., Kim, S., Seongkim, D., Pikhitsa, P.V., Choi, M. (2006). Parallel patterning of nanoparticles via electrodynamic focusing of charged aerosols. *Nature Nanotechnology*, 1, 117. <https://doi.org/10.1038/nnano.2006.94>
- Kim, B.J., Cheong, H., Hwang, B.H., Cha, H.J. Mussel-Inspired Protein Nanoparticles Containing Iron(III)-DOPA Complexes for pH-Responsive Drug Delivery (2015) *Angewandte Chemie - International Edition*, 54 (25), pp. 7318-732.
- Kim, M.Y., Lee, J. Coaxial nozzle electro spraying of polymer solutions: Use of dispersant flow (2011) *Polymer (Korea)*, 35 (3), pp. 254-259
- Kim, S.-Y., Yang, J., Kim, B., Park, J., Suh, J.-S., Huh, Y.-M., Haam, S., Hwang, J. Continuous coaxial electrohydrodynamic atomization system for water-stable wrapping of magnetic nanoparticles (2013) *Small*, 9 (13), pp. 2325-2330
- Kim, W., Kim, S.S. Multishell encapsulation using a triple coaxial electro spray system (2010) *Analytical Chemistry*, 82 (11), pp. 4644-4647
- Kiselev, P., Rosell, J., & Fenn, J. B. (1997). Determining the composition of liquid droplets in a gas of different composition. *Industrial & Engineering Chemistry Research*, 36(8), 3081–3084.
- Koo, S.Y., Cha, K.H., Song, D.-G., Chung, D., Pan, C.-H. Microencapsulation of peppermint oil in an alginate-pectin matrix using a coaxial electro spray system (2014) *International Journal of Food Science and Technology*, 49 (3), pp. 733-739.
- Ku, B. K. and Kim, S. S. (2002). Electro spray characteristics of highly viscous liquids, *J. Aerosol Sci.*, 33, 1361–1378.
- Kyritsis, D. C., Coriton, B., Faure, F., Roychoudhury, S., & Gomez, A. (2004). Optimization of a catalytic combustor using electro sprayed liquid hydrocarbons for mesoscale power generation. *Combustion and Flame*, 139(1–2), 77–89. <https://doi.org/10.1016/j.combustflame.2004.06.010>
- Laelorspoen, N., Wongsasulak, S., Yoovidhya, T., Devahastin, S. Microencapsulation of *Lactobacillus acidophilus* in zein-alginate core-shell microcapsules via electro spraying (2014) *Journal of Functional Foods*, 7 (1), pp. 342-349
- Landau, L.D. & Lifshitz, E.M. (1984) *Electrodynamics of continuous media*, Pergamon, Oxford.

- Lastow, O., & Balachandran, W. (2006). Numerical simulation of electrohydrodynamic (EHD) atomization. *Journal of Electrostatics*, 64(12), 850–859.
<http://doi.org/10.1016/j.elstat.2006.02.006>
- Lee, H., You, S., Woo, C. G., Lim, K., Jun, K., & Choi, M. (2009). Focused patterning of nanoparticles by controlling electric field induced particle motion. *Applied Physics Letters*, 94(5), 2009–2011. <https://doi.org/10.1063/1.3077158>
- Lee, Y.-H., Bai, M.-Y., Chen, D.-R. Multidrug encapsulation by coaxial tri-capillary electro-spray (2011) *Colloids and Surfaces B: Biointerfaces*, 82 (1), pp. 104-110.
- Lee, Y.-H., Mei, F., Bai, M.-Y., Zhao, S., Chen, D.-R. Release profile characteristics of biodegradable-polymer-coated drug particles fabricated by dual-capillary electro-spray (2010) *Journal of Controlled Release*, 145 (1), pp. 58-65.
- Li, C., Wang, F., Ge, P., Mao, Y., Wang, L. Anti-acute thrombogenic surface using coaxial electro-spraying coating for vascular graft application (2017) *Materials Letters*, 205, pp. 15-19.
- Li, F., Yin, X.-Y., Yin, X.-Z. Absolute and convective instability of a coaxial viscous liquid jet under both axial and radial electric fields (2016) *European Journal of Mechanics, B/Fluids*, 55, pp. 39-48.
- Li, F., Yin, X.-Y., Yin, X.-Z. Instability analysis of an inner-driving coaxial jet inside a coaxial electrode for the non-equipotential case (2008) *Journal of Electrostatics*, 66 (1-2), pp. 58-70.
- Li, F., Yin, X.-Y., Yin, X.-Z. Linear instability of a coflowing jet under an axial electric field (2006a) *Physical Review E - Statistical, Nonlinear, and Soft Matter Physics*, 74 (3), art. no. 036304.
- Li, F., Yin, X.-Y., Yin, X.-Z. Temporal linear instability analysis of an electrified coaxial jet with inner driving liquid inside a coaxial electrode (2006b) *Journal of Electrostatics*, 64 (10), pp. 690-698.
- Li, X.-Y., Zheng, Z.-B., Yu, D.-G., Liu, X.-K., Qu, Y.-L., Li, H.-L. Electro-sprayed spherical ethylcellulose nanoparticles for an improved sustained-release profile of anticancer drug (2017) *Cellulose*, pp. 1-14. Article in Press.
- Lim, L. K., Hua, J., Wang, C.-H., & Smith, K. A. (2011). Numerical simulation of cone-jet formation in electrohydrodynamic atomization. *AIChE Journal*, 57(1), 57–78.
<http://doi.org/10.1002/aic.12254>
- Liu, Z.-P., Cui, L., Yu, D.-G., Zhao, Z.-X., Chen, L. Electro-sprayed core-shell solid dispersions of acyclovir fabricated using an epoxy-coated concentric spray head (2014) *International Journal of Nanomedicine*, 9 (1), pp. 1967-1977.
- Lojewski, B., Yang, W., Duan, H., Xu, C., & Deng, W. (2013). Design, fabrication, and characterization of linear multiplexed electro-spray atomizers micro-machined from metal and polymers. *Aerosol Science and Technology*, 47(2), 146–152.
<https://doi.org/10.1080/02786826.2012.734936>
- López-Herrera, J.M., Barrero, A., López, A., Loscertales, I.G., Márquez, M. Coaxial jets generated from electrified Taylor cones. Scaling laws (2003) *Journal of Aerosol Science*, 34 (5), pp. 535-552.
- López-Herrera, J. M., Barrero, A., Boucard, A., Loscertales, I. G., & Márquez, M. (2004). An experimental study of the electro-spraying of water in air at atmospheric pressure. *Journal of the American Society for Mass Spectrometry*, 15(2), 253–259.
<https://doi.org/10.1016/j.jasms.2003.10.018>
- López-Herrera, J. M., Riesco-Chueca, P., & Gañán-Calvo, A. M. (2005). Linear stability analysis of axisymmetric perturbations in imperfectly conducting liquid jets. *Physics of Fluids*, 17(3), 034106 (22pp). <https://doi.org/10.1063/1.1863285>
- López Urdiales, J. M. (2004). Progress in colloid propulsion. Massachusetts Institute of Technology. Retrieved from <http://hdl.handle.net/1721.1/28891>
- Loscertales, I. G. and Fernández de la Mora, J. (1995). Experiments on the kinetics of field evaporation of small ions from droplets. *J. Chem. Phys.*, 103(12), 5041-5060.
<https://doi.org/10.1063/1.470591>

- Loscertales, I.G., Barrero, A., Guerrero, I., Cortijo, R., Marquez, M., Gañán-Calvo, A.M. Micro/nano encapsulation via electrified coaxial liquid jets (2002) *Science*, 295 (5560), pp. 1695-1698.
- Luo, C.J., Edirisinghe, M. Core-liquid-induced transition from coaxial electrospray to electrospinning of low-viscosity poly(lactide-co-glycolide) sheath solution (2014) *Macromolecules*, 47 (22), pp. 7930-7938.
- Maißer, A., Attoui, M. B., Gañán-Calvo, A. M. and Szymanski, W. W. (2013). Electrohydrodynamic generation of monodisperse nanoparticles in the sub-10 nm size range from strongly electrolytic salt solutions: Governing parameters of scaling laws. *J. Nanopart. Res.*, 15(1). <https://doi.org/10.1007/s11051-012-1318-2>
- Marginean, I., Parvin, L., Heffernan, L., & Vertes, A. (2004). Flexing the electrified meniscus: The birth of a jet in electrosprays. *Analytical Chemistry*, 76(14), 4202–4207. <http://doi.org/10.1021/ac049817r>
- Marginean, I., Nemes, P., & Vertes, A. (2007). A stable regime in electrosprays. *Physical Review E - Statistical, Nonlinear, and Soft Matter Physics*, 76(2), 1–6. <http://doi.org/10.1103/PhysRevE.76.026320>
- Marín, A.G., Loscertales, I.G., Barrero, A. Conical tips inside cone-jet electrosprays (2008) *Physics of Fluids*, 20 (4), art. no. 042102
- Marín, Á.G., Loscertales, I.G., Márquez, M., Barrero, A. Simple and double emulsions via coaxial jet electrosprays (2007) *Physical Review Letters*, 98 (1), art. no. 014502
- Mei, F., Chen, D.-R. Investigation of compound jet electrospray: Particle encapsulation (2007) *Physics of Fluids*, 19 (10), art. no. 103303
- Melcher, J. R., & Taylor, G. I. (1969). Electrohydrodynamics - A Review of role of interfacial shear stresses. *Annual Review of Fluid Mechanics*, 1, 111–146. <http://doi.org/10.1146/annurev.fl.01.010169.000551>
- Melcher, J. R., & Warren, E. P. (1971). Electrohydrodynamics of a current-carrying semi-insulating jet. *Journal of Fluid Mechanics*, 47, 127-143. <http://doi.org/10.1017/S0022112071000971>
- Miller, R. S., Harstad, K., & Bellan, J. (1998). Evaluation of equilibrium and non-equilibrium evaporation for many-droplet gas-liquid flow simulations. *International Journal of Multiphase Flow*, 24(6), 1025–1055. [https://doi.org/10.1016/S0301-9322\(98\)00028-7](https://doi.org/10.1016/S0301-9322(98)00028-7)
- Morozov, V. N., & Morozova, T. Y. (1999). Electrospray deposition as a method for mass fabrication of mono- and multicomponent microarrays of biological and biologically active substances. *Analytical Chemistry*, 71(15), 3110–3117. <https://doi.org/10.1021/ac981412h>
- Mou, F., Xu, L., Ma, H., Guan, J., Chen, D.-R., Wang, S. Facile preparation of magnetic γ -Fe₂O₃/TiO₂ Janus hollow bowls with efficient visible-light photocatalytic activities by asymmetric shrinkage (2012) *Nanoscale*, 4 (15), pp. 4650-4657.
- Naqwi, A. A. (1994). In situ measurement of submicron droplets in electrosprays using a planar phase Doppler system. *Journal of Aerosol Science*, 25(6), 1201–1211. [https://doi.org/10.1016/0021-8502\(94\)90209-7](https://doi.org/10.1016/0021-8502(94)90209-7)
- Naqwi, A., Hartman, R. P., & Marijnissen, J. C. M. (1996). Basic studies of electrohydrodynamic atomization process using phase Doppler measurement technique. *Particle & Particle Systems Characterization*, 13, 143–149. <https://doi.org/10.1002/ppsc.19960130213>
- Nemes, P., Marginean, I., & Vertes, A. (2007). Spraying mode effect on droplet formation and ion chemistry in electrosprays. *Analytical Chemistry*, 79(8), 3105–3116. <https://doi.org/10.1021/ac062382i>
- Nguyen, D. N., Clasen, C., & Van den Mooter, G. (2016). Pharmaceutical applications of electrospinning. *Journal of Pharmaceutical Sciences*, 105(9), 2601–2620. <http://doi.org/10.1016/j.xphs.2016.04.024>
- Notz, P. K., & A., Basaran, O. (1999). Dynamics of drop formation in an electric field. *Journal of Colloid and Interface Science*, 213, 218–237. <http://doi.org/10.1006/jcis.1999.6136>

- Oh, H., Kim, K., & Kim, S. (2008). Characterization of deposition patterns produced by twin-nozzle electrospray. *Journal of Aerosol Science*, 39(9), 801–813.
<https://doi.org/10.1016/j.jaerosci.2008.05.003>
- Okuyama, K., & Lenggoro, W. W. (2003). Preparation of nanoparticles via spray route. *Chemical Engineering Science*, 58(3–6), 537–547. [http://doi.org/10.1016/S0009-2509\(02\)00578-X](http://doi.org/10.1016/S0009-2509(02)00578-X)
- Olumee, Z., Callahan, J., & Vertes, A. (1998). Droplet dynamics changes in electrostatic sprays of methanol-water mixtures. *The Journal of Physical Chemistry A*, 102, 9154–9160.
<https://doi.org/10.1021/jp982027z>
- Olvera-Trejo, D., Velásquez-García, L.F. Additively manufactured MEMS multiplexed coaxial electrospray sources for high-throughput, uniform generation of core-shell microparticles (2016) *Lab on a Chip*, 16 (21), pp. 4121-4132.
- Ondimu, O. M., Ganesan, V. A., Gatari, M. J., Marijnissen, J. C. M., & Agostinho, L. L. F. (2017). Modeling simple-jet mode electrohydrodynamic-atomization droplets' trajectories and spray pattern for a single nozzle system. *Journal of Electrostatics*, 89, 77–87.
<https://doi.org/10.1016/j.elstat.2017.08.001>
- Pantano, C., Gañán-Calvo, A. M., & Barrero, A. (1994). Zeroth-order, electrohydrostatic solution for electro spraying in cone-jet mode. *Journal of Aerosol Science*, 25(6), 1065–1077. [https://doi.org/http://dx.doi.org/10.1016/0021-8502\(94\)90202-X](https://doi.org/http://dx.doi.org/10.1016/0021-8502(94)90202-X)
- Park, H., Kim, K., & Kim, S. (2004). Effects of a guard plate on the characteristics of an electrospray in the cone-jet mode. *Journal of Aerosol Science*, 35(11), 1295–1312.
<https://doi.org/10.1016/j.jaerosci.2004.05.012>
- Park, I., Hong, W. S., Kim, S. B., & Kim, S. S. (2017). Experimental investigations on characteristics of stable water electrospray in air without discharge. *Phys. Rev. E*, 95(6), 63110. <https://doi.org/10.1103/PhysRevE.95.063110>
- Park, I., Kim, W., Kim, S.S. Multi-jet mode electrospray for non-conducting fluids using two fluids and a coaxial grooved nozzle (2011a) *Aerosol Science and Technology*, 45 (5), pp. 629-634
- Park, S., Hwang, S., Lee, J. PH-responsive hydrogels from moldable composite microparticles prepared by coaxial electro-spray drying (2011b) *Chemical Engineering Journal*, 169 (1-3), pp. 348-357.
- Pfeifer, R. J., & Hendricks, C. D. J. (1968). Parametric studies of electrohydrodynamic spraying. *AIAA JOURNAL*, 6(3), 496–502.
- Rayleigh, J. W. S. (1882). In *The Theory of Sound*, volume II, Dover, New York, 1945. p. 374. Unabridged republication of the second edition of 1896.
- Reneker, D. H., & Yarin, A. L. (2008). Electrospinning jets and polymer nanofibers. *Polymer*, 49(10), 2387–2425. <https://doi.org/10.1016/j.polymer.2008.02.002>
- Riboux, G., Marín, Á. G., Loscertales, I. G., & Barrero, A. (2011). Whipping instability characterization of an electrified visco-capillary jet. *Journal of Fluid Mechanics*, 671, 226–253. <http://doi.org/10.1017/S0022112010005586>
- Rietveld, I. B., Kobayashi, K., Yamada, H., & Matsushige, K. (2006). Morphology control of poly(vinylidene fluoride) thin film made with electrospray. *Journal of Colloid and Interface Science*, 298(2), 639–651. <https://doi.org/10.1016/j.jcis.2005.12.028>
- Rodríguez-Pérez, D., Castillo, J. L., & Antoranz, J. C. (2005). Relationship between particle deposit characteristics and the mechanism of particle arrival. *Physical Review E - Statistical, Nonlinear, and Soft Matter Physics*, 72(2), 1–9.
<https://doi.org/10.1103/PhysRevE.72.021403>
- Rosell, J. (1994). *Size Characterization in Electrosprays of Submicron Droplets*. PhD Thesis. Yale University.
- Rosell-Llompарт, J., & Fernández de la Mora, J. (1994). Generation of monodisperse droplets 0.3 to 4 μm in diameter from electrified cone-jets of highly conducting and viscous liquids. *Journal of Aerosol Science*, 25(6), 1093–1119.
[http://doi.org/http://dx.doi.org/10.1016/0021-8502\(94\)90204-6](http://doi.org/http://dx.doi.org/10.1016/0021-8502(94)90204-6)

- Sample, S. B., & Bollini, R. (1972). Production of liquid aerosols by harmonic electrical spraying. *Journal of Colloid and Interface Science*, 41(2), 185–193. [http://doi.org/10.1016/0021-9797\(72\)90107-5](http://doi.org/10.1016/0021-9797(72)90107-5)
- Sarkar, K., Hoos, P., & Urias, A. (2013). Numerical Simulation of Formation and Distortion of Taylor Cones. *Journal of Nanotechnology in Engineering and Medicine*, 3(4), 041001 (10pp). <http://doi.org/10.1115/1.4023243>
- Saville, D. A. (1997). Electrohydrodynamics: The Taylor-Melcher leaky dielectric model. *Annual Review of Fluid Mechanics*, 29(1), 27–64. <https://doi.org/10.1146/annurev.fluid.29.1.27>
- Scheideler, W. J. and Chen, C. H. (2014). The minimum flow rate scaling of Taylor cone-jets issued from a nozzle. *Appl. Phys. Lett.*, 104(2). <http://doi.org/10.1063/1.4862263>
- Sen, A. K., Darabi, J., & Knapp, D. R. (2011). Analysis of Droplet Generation in Electrospray Using a Carbon Fiber Based Microfluidic Emitter. *Journal of Fluids Engineering*, 133(7), 071301 (8pp). <http://doi.org/10.1115/1.4004325>
- Sen, A. K., Darabi, J., Knapp, D. R., & Liu, J. (2006). Modeling and characterization of a carbon fiber emitter for electrospray ionization. *Journal of Micromechanics and Microengineering*, 16(3), 620–630. <http://doi.org/10.1088/0960-1317/16/3/018>
- Shorey, J. D., & Michelson, D. (1970). On the mechanism of electrospraying. *Nuclear Instruments and Methods*, 82(Supplement C), 295–296. [http://doi.org/https://doi.org/10.1016/0029-554X\(70\)90368-X](http://doi.org/https://doi.org/10.1016/0029-554X(70)90368-X)
- Si, T., Zhang, L., Li, G., Roberts, C.J., Yin, X., Xu, R. Experimental design and instability analysis of coaxial electrospray process for microencapsulation of drugs and imaging agents (2013) *Journal of Biomedical Optics*, 18 (7), art. no. 075003,
- Si, T., Zhang, L., Li, G., Xu, R. Novel coaxial atomization processes for microfabrication of multi-layered biodegradable microcapsules (2012) *Progress in Biomedical Optics and Imaging - Proceedings of SPIE*, 8553, art. no. 85531H.
- Smith, D. P. H. (1986). The electrohydrodynamic atomization of liquids. *IEEE Transactions on Industry Applications*, IA-22(3), 527–535. <http://doi.org/10.1109/TIA.1986.4504754>
- Smith, K. L., Alexander, M. S. and Stark, J. P. W. (2006). The role of molar conductivity in electrospray cone-jet mode current scaling. *J. Appl. Phys.*, 100(1). <http://doi.org/10.1063/1.2210169>
- Snarski, S. R., & Dunn, P. F. (1991). Experiments characterizing the interaction between two sprays of electrically charged liquid droplets. *Experiments in Fluids*, 11(4), 268–278. <https://doi.org/10.1007/BF00192755>
- Sofokleous, P., Lau, W.K., Edirisinghe, M., Stride, E. The effect of needle tip displacement in co-axial electrohydrodynamic processing (2016) *RSC Advances*, 6 (79), pp. 75258-75268.
- Srivastava, Y., Loscertales, I., Marquez, M., Thorsen, T. Electrospinning of hollow and core/sheath nanofibers using a microfluidic manifold, *Microfluidics and Nanofluidics* 4, 245-250 (2007)
- Tang, H. Bin, Qin, C. J., & Liu, Y. (2011). Characterization of colloid thruster beams and plumes. *Journal of Aerosol Science*, 42(2), 114–126. <https://doi.org/10.1016/j.jaerosci.2010.12.002>
- Tang, K., & Gomez, A. (1994). On the structure of an electrostatic spray of monodisperse droplets. *Physics of Fluids*, 6(7), 2317–2332. <https://doi.org/10.1063/1.868182>
- Tang, K., & Gomez, A. (1995). Generation of monodisperse water droplets from electrosprays in a corona-assisted cone-jet mode. *Journal of Colloid and Interface Science*, 175(2), 326–332. <https://doi.org/10.1006/jcis.1995.1464>
- Tang, K., & Gomez, A. (1996). Monodisperse electrosprays of low electric conductivity liquids in the cone-jet mode. *Journal of Colloid and Interface Science*, 184(2), 500–511.
- Taylor, G. (1964). Disintegration of water drops in an electric field. *Proceedings of the Royal Society A: Mathematical, Physical and Engineering Sciences*, 280(1382), 383–397. <https://doi.org/10.1098/rspa.1964.0151>

- Taylor, G. (1969). Electrically driven jets. *Proceedings of the Royal Society of London. A. Mathematical and Physical Sciences*, 313(1515), 453–475.
<https://doi.org/10.1098/rspa.1969.0205>
- Velásquez-García, L. F., Akinwande, A. I., & Martínez-Sánchez, M. (2006). A planar array of micro-fabricated electrospray emitters for thruster applications. *Journal of Microelectromechanical Systems*, 15(5), 1272–1280.
<http://doi.org/10.1109/JMEMS.2006.879710>
- Verdigh, V., & Lauer, K. F. (1964). Equipment for electrospraying. *Nuclear Instruments and Methods*, 31(2), 355–356. [http://doi.org/10.1016/0029-554X\(64\)90190-9](http://doi.org/10.1016/0029-554X(64)90190-9)
- Verdoold, S., Agostinho, L. L. F., Yurteri, C. U., & Marijnissen, J. C. M. (2014). A generic electrospray classification. *Journal of Aerosol Science*, 67, 87–103.
- Wang, Y., Yang, X., Liu, W., Zhang, F., Cai, Q., Deng, X. Controlled release behaviour of protein-loaded microparticles prepared via coaxial or emulsion electrospray (2013) *Journal of Microencapsulation*, 30 (5), pp. 490-497.
- Wang, Z., Xia, L. and Zhan, S. (2017). Experimental study on electrohydrodynamics (EHD) spraying of ethanol with double-capillary. *Appl. Therm. Eng.*, 120, 474–483.
<http://doi.org/10.1016/j.applthermaleng.2017.04.013>
- Wei, W., Gu, Z., Wang, S., Zhang, Y., Lei, K., & Kase, K. (2013). Numerical simulation of the cone-jet formation and current generation in electrostatic spray - Modeling as regards space charged droplet effect. *Journal of Micromechanics and Microengineering*, 23(1).
<http://doi.org/10.1088/0960-1317/23/1/015004>
- Wilhelm, O., Mädler, L., & Pratsinis, S. E. (2003). Electrospray evaporation and deposition. *Journal of Aerosol Science*, 34(7), 815–836. [https://doi.org/10.1016/S0021-8502\(03\)00034-X](https://doi.org/10.1016/S0021-8502(03)00034-X)
- Wilhelm, O., & Mädler, L. (2006). Cone-jet and multijet electrosprays: Transport and evaporation. *Atomization and Sprays*, 16(1), 83–102.
<https://doi.org/10.1615/AtomizSpr.v16.i1.60>
- Wilhelm, O., Pratsinis, S. E., Perednis, D., & Gauckler, L. J. (2005). Electrospray and pressurized spray deposition of yttria-stabilized zirconia films. *Thin Solid Films*, 479(1–2), 121–129. <https://doi.org/10.1016/j.tsf.2004.11.206>
- Wortmann, A., Kistler-Momotova, A., Zenobi, R., Heine, M. C., Wilhelm, O., & Pratsinis, S. E. (2007). Shrinking droplets in electrospray ionization and their influence on chemical equilibria. *Journal of the American Society for Mass Spectrometry*, 18(3), 385–393.
<https://doi.org/10.1016/j.jasms.2006.10.010>
- Wu, Y., Fei, Z., Lee, L.J., Wyslouzil, B.E. Coaxial electrohydrodynamic spraying of plasmid DNA/polyethylenimine (PEI) polyplexes for enhanced nonviral gene delivery (2010) *Biotechnology and Bioengineering*, 105 (4), pp. 834-841.
- Wu, Y., Liao, I.-C., Kennedy, S.J., Du, J., Wang, J., Leong, K.W., Clark, R.L. Electrosprayed core-shell microspheres for protein delivery (2010) *Chemical Communications*, 46 (26), pp. 4743-4745
- Wu, Y., Yu, B., Jackson, A., Zha, W., Lee, L.J., Wyslouzil, B.E. Coaxial electrohydrodynamic spraying: A novel one-step technique to prepare oligodeoxynucleotide encapsulated lipoplex nanoparticles (2009) *Molecular Pharmaceutics*, 6 (5), pp. 1371-1379.
- Xi, J., Zhang, Q., Myers, D., Sun, Y., Cao, G. Hollow hemispherical titanium dioxide aggregates fabricated by coaxial electrospray for dye-sensitized solar cell application (2012) *Journal of Nanophotonics*, 6 (1), art. no. 063519
- Xie, J., Jiang, J., Davoodi, P., Srinivasan, M. P., & Wang, C. H. (2015). Electrohydrodynamic atomization: A two-decade effort to produce and process micro-/nanoparticulate materials. *Chemical Engineering Science*, 125, 32–57. <http://doi.org/10.1016/j.ces.2014.08.061>
- Xu, Q., Qin, H., Yin, Z., Hua, J., Pack, D. W., & Wang, C. H. (2013). Coaxial electrohydrodynamic atomization process for production of polymeric composite microspheres. *Chemical Engineering Science*, 104, 330–346.
<http://doi.org/10.1016/j.ces.2013.09.020>

- Xu, S., Xu, Q., Zhou, J., Wang, J., Zhang, N., Zhang, L. Preparation and characterization of folate-chitosan-gemcitabine core-shell nanoparticles for potential tumor-targeted drug delivery (2013) *Journal of Nanoscience and Nanotechnology*, 13 (1), pp. 129-138.
- Xu, Y., Hanna, M.A. Morphological and structural properties of two-phase coaxial jet electrosprayed BSA-PLA capsules (2008) *Journal of Microencapsulation*, 25 (7), pp. 469-477
- Yamashita, M., & Fenn, J. B. (1984). Electrospray ion source. Another variation on the free-jet theme. *The Journal of Physical Chemistry*, 88(20), 4451–4459.
<http://doi.org/10.1021/j150664a002>
- Yan, W.-C., Davoodi, P., Tong, Y. W., & Wang, C.-H. (2016). Computational study of core-shell droplet formation in coaxial electrohydrodynamic atomization process. *AIChE Journal*, 62(12), 4259–4276. <http://doi.org/10.1002/aic.15361>
- Yan, W.-C., Tong, Y.W., Wang, C.-H. Coaxial electrohydrodynamic atomization toward large scale production of core-shell structured microparticles (2017) *AIChE Journal*, . Article in Press.
- Yang, W., Lojewski, B., Wei, Y., & Deng, W. (2012). Interactions and deposition patterns of multiplexed electrosprays. *Journal of Aerosol Science*, 46, 20–33.
<https://doi.org/10.1016/j.jaerosci.2011.11.004>
- Yang, H., Qiao, X., Hong, W., Dong, L. Core-shell microcapsules with embedded microactuators for regulated release (2013) *Journal of Microelectromechanical Systems*, 22 (3), art. no. 6365219, pp. 509-518.
- Yoo, J.Y., Kim, M., Lee, J. Electrospraying of micro/nano particles for protein drug delivery (2007) *Polymer (Korea)*, 31 (3), pp. 215-220.
- Yoon, K.H., Unyong, J., Eun, C.C. Production of uniform-sized polymer core-shell microcapsules by coaxial electrospraying (2008) *Langmuir*, 24 (6), pp. 2446-245
- You, S., & Choi, M. (2007). Numerical simulation of microscopic motion and deposition of nanoparticles via electrodynamic focusing. *Journal of Aerosol Science*, 38(11), 1140–1149. <https://doi.org/10.1016/j.jaerosci.2007.08.002>
- Yurteri, C. U., Hartman, R. P. A., & Marijnissen, J. C. M. (2010). Producing pharmaceutical particles via electrospraying with an emphasis on nano and nano structured particles - A review. *KONA Powder and Particle Journal*, 28, 91–115.
<http://doi.org/10.14356/kona.2010010>
- Zamani, M., Prabhakaran, M.P., Ramakrishna, S. Advances in drug delivery via electrospun and electrosprayed nanomaterials (2013) *International Journal of Nanomedicine*, 8, pp. 2997-3017
- Zamani, M., Prabhakaran, M.P., Thian, E.S., Ramakrishna, S. Controlled delivery of stromal derived factor-1 α from poly lactic-co-glycolic acid core-shell particles to recruit mesenchymal stem cells for cardiac regeneration (2015) *Journal of Colloid and Interface Science*, 451, pp. 144-152.
- Zamani, M., Prabhakaran, M.P., Thian, E.S., Ramakrishna, S. Protein encapsulated core-shell structured particles prepared by coaxial electrospraying: Investigation on material and processing variables (2014) *International Journal of Pharmaceutics*, 473 (1-2), pp. 134-143.
- Zeleny, J. (1907) The discharge of electricity from pointed conductors differing in size. *Phys. Rev.*, 25, 303-333.
- Zeleny, J. (1914) The electrical discharge from liquid points, and a hydrostatic method of measuring the electric intensity at their surfaces. *Phys. Rev.*, 3, 69-91.
- Zeleny, J. (1915) On the conditions of instability of electrified drops, with applications to the electrical discharge from liquid points. *Proc. Phil. Cam. Soc.*, 18, 71-83.
- Zeleny, J. (1917) Instability of electrified liquid surfaces. *Phys. Rev.*, 10, 1-6.
- Zeleny, J. (1920) Electrical discharges from pointed conductors", *Phys. Rev.*, 16, 102-125, 1920.
- Zeleny, J. (1935) The role of surface instability in electrical discharges from drops of alcohol and water in air at atmospheric pressure", *J. Franklin Inst.*, 219, 659-675.

- Zhang, C., Yao, Z.-C., Ding, Q., Choi, J.J., Ahmad, Z., Chang, M.-W., Li, J.-S. Tri-Needle Coaxial Electro spray Engineering of Magnetic Polymer Yolk-Shell Particles Possessing Dual-Imaging Modality, Multiagent Compartments, and Trigger Release Potential (2017) *ACS Applied Materials and Interfaces*, 9 (25), pp. 21485-21495.
- Zhang, L., Huang, J., Si, T., Xu, R.X. Coaxial electro spray of microparticles and nanoparticles for biomedical applications (2012a) *Expert Review of Medical Devices*, 9 (6), pp. 595-612.
- Zhang, L., Yan, Y., Mena, J., Sun, J., Letson, A., Roberts, C., Zhou, C., Chai, X., Ren, Q., Xu, R. Electro spray of multifunctional microparticles for image-guided drug delivery (2012b) *Progress in Biomedical Optics and Imaging - Proceedings of SPIE*, 8233, art. no. 823303
- Zhang, Q., Wang, L., Wei, Z., Wang, X., Long, S., Yang, J. A new simple method to prepare hollow PES microspheres (2012c) *Colloid and Polymer Science*, 290 (13), pp. 1257-1263.
- Zhang, S., Kawakami, K., Yamamoto, M., Masaoka, Y., Kataoka, M., Yamashita, S., Sakuma, S. Coaxial electro spray formulations for improving oral absorption of a poorly water-soluble drug (2011) *Molecular Pharmaceutics*, 8 (3), pp. 807-813
- Zhao, S., Agarwal, P., Rao, W., Huang, H., Zhang, R., Liu, Z., Yu, J., Weisleder, N., Zhang, W., He, X. Coaxial electro spray of liquid core-hydrogel shell microcapsules for encapsulation and miniaturized 3D culture of pluripotent stem cells (2014) *Integrative Biology (United Kingdom)*, 6 (9), pp. 874-884.
- Zhou, S., & Cook, K. D. (2000). Probing solvent fractionation in electro spray droplets with laser-induced fluorescence of a solvatochromic dye. *Analytical Chemistry*, 72(5), 963–969. <https://doi.org/10.1021/ac990912n>
- Zhu, W., Lee, S.-J., Castro, N.J., Yan, D., Keidar, M., Zhang, L.G. Synergistic Effect of Cold Atmospheric Plasma and Drug Loaded Core-shell Nanoparticles on Inhibiting Breast Cancer Cell Growth (2016) *Scientific Reports*, 6, art. no. 21974